Sirte University

Faculty of Science

Department of Chemistry

Investigation of Solvent Effects on Spectroscopic and Photochemical Properties of Ruthenium (II) Polypyridyl Complexes

Student Name

Hadeel Ali Mohammed Alsayd

Under Supervision

Professor Dr. Hamid. M. Younis

Dr. Salima . M. Hussein Mohamed

Thesis Submitted in Partial Fulfilment of the Requirements for the Degree Master of Science in Chemistry

Academic Year 2024-2025

جامعـــــة ســـــرت
كليـــــة العـــلوم
قســـم الكيميـاء

دراسة تأثير بعض المذيبات على الخواص الطيفية والكيميائية الضوئية لمعقدات الروثينيوم (II) بولي بيريديل

إعداد الطالبة:

هديل علي محمد الصيد

تحت إشراف:

ا. د. احميد محمد يونس

د. سليمة مفتاح حسين

قدمت هذه الرسالة كأحد متطلبات الحصول على درجة الإجازة العالية (الماجستير)
في العلوم تخصص كيمياء

العام الجامعي 2024-2025

Declaration

I confirm that the work contained in this thesis, unless otherwise referenced, is the researcher's own work and has not been previously submitted to meet the requirements for an award at this university or any other higher education or research institution. I furthermore cede copyright of this thesis in favor of the University of Sirte.

Student name: Hadeel Ali Mohammed Alsayd

Signature: .....

Date: 15 /4/ 2025

إقرار

أقرّ بأن العمل الوارد في هذه الأطروحة، ما لم يُذكر خلاف ذلك، هو عمل الباحث الأصلي ولم يُقدَّم مسبقًا لاستيفاء متطلبات أي درجة علمية في هذه الجامعة أو أي مؤسسة أخرى للتعليم العالي أو البحث العلمي. علاوة على ذلك، أتنازل عن حقوق الطبع والنشر لهذه الأطروحة لصالح جامعة سرت.

اسم الطالبة: هديل علي محمد الصيد

التوقيع:

التاريخ: 15 / 4 / 2025

وزارة التعليم العالي والبحث العلمي

جامعة سرت

إدارة الدراسات العليا والتدريب

كلية العلوم – قسم الكيمياء

برنامج الماجستير

قدمت هذه الرسالة كأحد متطلبات الحصول على درجة الإجازة العالية الماجستير بعنوان

دراسة تأثير بعض المذيبات على الخواص الطيفية والكيميائية الضوئية لمعقدات الروثينيوم (II) بولي بيريديل

إعداد الطالبة: هديل علي محمد الصيد

لجنة المناقشة:

الاسم	الدرجة العلمية	الصفة	التوقيع
ا. د. احميد محمد يونس	أستاذ	المشرف/ رئيس اللجنة	
د. سليمة مفتاح حسين	أستاذ مشارك	مشرف مساعد	تغيب لعارض صحي
ا. د. عبد السلام الصالحين محمد	أستاذ	ممتحن داخلي	
ا. د. عادل امحمد الأجطل	أستاذ	ممتحن خارجي	

د. فتحية عبد الجواد موسى

رئيس قسم الكيمياء

ا. د. احميد محمد يونس

مدير مكتب الدراسات العليا والتدريب

د. اشرف مصطفى ابوسنينه

عميد الكلية

Acknowledgement

First of all, I would like to express my gratitude to Prof. Dr. Hamid Mohamed Younis my supervisor, for the opportunity he gave me his guide and experience during these last six months to complete my thesis at Sirte University.

Special thanks to all my family for their patience during my study.

Hadeel Ali Mohammed

Contents

List of tables

List of Figures

List of abbreviations

Abbreviation	Meaning
B	Bridging ligand
Cat	Catalytic center
C_M	Mass transfer coefficient in mobile phase
C_S	Mass transfer coefficient in stationary phase
CT	Charge transfer
DCU	Dublin City University
DFT	Density functional theory
EPR	Extended producer responsibility
ET	Energy transfer
FRET	Förster energy transfer
GPC	Gel permeation chromatography
^{1}H-NMR	Proton nuclear magnetic resonance
HOMO	Highest occupied molecular orbital
HPLC	High performance liquid chromatography
IEC	Ion exchange chromatography
IL	Intraligand
Irr	Irradiation
ISC	Intersystem crossing
LC	Liquid chromatography
LED	Light emitting diodes
LMCT	Ligand to metal charge transfer
LUMO	Lowest unoccupied molecular orbital
MC	Metal centered band
^{3}MC	Triplet metal centered
MET	Marcus Electron Transfer Theory
MLCT	Metal to ligand charge transfer
^{3}MLCT	Triplet metal to ligand charge transfer

Mos	Metal oxide semiconductor
PHE	Photo hydrogen evolving process
PS	Photosensitizer
Rs	Resolution
RSD	Relative standard deviation
SAX	Strong anion exchanger
SCX	Strong cation exchanger
SEC	Size exclusion chromatography
SPE	Solid phase extraction
Tbbpy	4,4'-tert-butyl-2,2'-bipyridine
TD-DFT	Time dependent density functional theory
TEA	Triethyl amine
TOF	Turnover frequency
TON	Turnover number
Tpphz	Tetrapyrido[3,2-a:2',3'-c:2",3'"- j] phenazine
UV- Vis	Ultraviolet – Visible
WAX	Weak anion exchanger
WCX	Weak cation exchanger

Abstract

This study investigates the effect of various solvents on the spectroscopic and photochemical properties of ruthenium (II) polypyridyl complexes, which are widely used in solar energy conversion and hydrogen production. The research aims to assess the stability, electronic transitions, and photochemical behavior of these complexes under irradiation, utilizing advanced analytical techniques such as high-performance liquid chromatography (HPLC) and UV-Vis spectroscopy.

In Chapter 1, a theoretical background is provided on the fundamental photophysical and electrochemical properties of ruthenium (II) polypyridyl complexes, focusing on metal-to-ligand charge transfer (MLCT) mechanisms and their role in photocatalysis. The impact of solvent interactions on modifying photodynamic behavior is analyzed to optimize catalytic efficiency.

In Chapter 2, the experimental methodology is outlined, where ruthenium (II) complexes were studied in different solvents, including acetonitrile (CH_3CN), methanol (CH_3OH), and dimethyl sulfoxide (DMSO). UV-Vis spectroscopy and HPLC techniques were employed to analyze stability and photochemical reactivity under various solvent conditions.

In Chapter 3, key experimental findings revealed significant MLCT peak shifts upon irradiation. The complex $[(tbbpy)_2Ru(tpphz)(PtI_2)_2]$ exhibited the highest molar absorptivity in acetonitrile and methanol, with the MLCT transition shifting from 486 nm to 441 nm over 24 hours, indicating solvent-induced ligand exchange and enhanced charge transfer. The presence of platinum iodide (PtI_2) improved photocatalytic efficiency, leading to increased hydrogen production (TON = 276), demonstrating the role of ligand selection in optimizing performance and stability. The molar absorptivity variations remained within acceptable experimental limits, with standard deviations ranging between ±1.1 and ±1.5 nm, and relative standard deviation (RSD) values below 3%, ensuring high measurement precision and reliability. At a 95% confidence level, the observed wavelength shifts ranged from 438.9 to 446.5 nm, further supporting the accuracy and reproducibility of the experimental data. These findings confirm that solvent type and ligand selection play a critical role in enhancing the efficiency of ruthenium (II) complexes in photocatalytic applications. High-polarity solvents stabilize charge transfer states, improving catalytic performance.

However, challenges such as solvent-induced ligand exchange were observed, which may impact long-term stability. Future research should explore alternative ligand designs that enhance stability and charge transfer properties. Additionally, investigating the impact of new solvent environments and integrating these complexes into multi-component catalytic systems could further improve efficiency and real-world applicability.

Keywords: ***(Ruthenium (II) polypyridine complexes, Photocatalysis, MLCT, Solar-driven hydrogen production, Solvent polarity effects, Photostability)***

CHAPTER 1

Chemistry of Ruthenium (II) Complexes and Their Applications in Photonic Devices

1. Introduction

Ruthenium (II) polypyridine complexes, such as $Ru(bpy)_3^{2+}$, have been extensively studied over the past four decades. Since the discovery of $[Ru(bpy)_3]\ Cl_2$ as a photostable and highly luminescent molecule exhibiting emission derived from triplet metal-to-ligand charge transfer (^{3}MLCT) (Paris & Brandt, 1959; Njabon, 2013), research has focused on their unique ground and excited-state properties.

Various research groups have explored the unusual electronic properties of Ru (II) polypyridyl complexes. These complexes are among the few transition metal complexes that exhibit strong luminescence in solution at room temperature and possess excellent photosensitization capacity (PS capacity) for electron- and energy-transfer processes. Their behavior has led to fundamental discussions on factors governing excited-state dynamics (Kalyanasundaram, 1982).

In air-saturated aqueous solutions, the excited-state lifetime of Ru (II) polypyridine complexes is approximately 300 nanoseconds. While this is relatively short, it is sufficient for redox reactions to proceed efficiently in the excited state. Additionally, ruthenium compounds are thermally stable across different oxidation states (Njabon, 2013).

The primary advantages of luminescent transition metal complexes include their high photostability, long-lived phosphorescence, which enables time-resolved detection, and significant Stokes shifts that reduce self-quenching. Furthermore, the cellular uptake of these metal complexes can be evaluated using inductively coupled plasma mass spectrometry (Kenneth, 2015).

Ru (II) polypyridyl complexes have been utilized in various applications, including electrochemical sensors, molecular electronics, oxygen sensors, molecular wires, bioprobes, and molecular machines (Johannes & Mary, 2010).

The widespread use of fossil fuels has led to significant environmental concerns, including an increase in the greenhouse effect. As a result, there is a growing focus on renewable energy sources. Solar energy, being abundant and cost-effective, has garnered significant interest. Developing devices that efficiently absorb sunlight and convert it into fuel or electricity in an economically, technically, and environmentally

sustainable manner is crucial. Artificial photosynthesis, which employs solar photocatalysts to convert water and CO_2 into fuels, is a promising approach. This study reviews advancements in hybrid molecular photocatalyst systems immobilized on semiconductor surfaces for solar fuel production through water oxidation and CO_2 reduction, as well as the challenges associated with their potential applications (Sinval et al., 2019; James & Gary, 2006; Nathan & Daniel, 2006).

The availability of diimine ligands and various synthesis and separation techniques allows for the design of complexes with tailored properties. In optical systems, Ru (II) and Os (II) diimine complexes serve as photo-oxidants and reductants. These complexes find applications in photochemical energy storage, solar energy conversion, and molecular devices. Additionally, the synthesis of symmetrical and asymmetrical polynuclear complexes and mixed-metal polynuclear complexes has expanded their role in supramolecular chemistry (Wilkinson et al., 1987; Scandola & Balzani, 1991; Balzani, 1987).

Ruthenium (II) polypyridine complexes have garnered significant attention due to their remarkable photophysical and electrochemical characteristics. These complexes exhibit strong metal-to-ligand charge transfer (MLCT) transitions, making them highly suitable for applications in artificial photosynthesis, solar energy conversion, and molecular electronic devices. A prominent example is tris(2,2′-bipyridine) ruthenium (II) chloride ($Ru(bpy)_3Cl_2$), which is widely recognized as a benchmark in photoredox catalysis and dye-sensitized solar cells (Kalyanasundaram, 1982).

1.1 Applications in Photocatalysis and Solar Energy

With the growing demand for sustainable energy solutions, research on photocatalytic hydrogen production and CO_2 reduction using ruthenium-based complexes has expanded significantly. Dinuclear Ru/Pt complexes have demonstrated high efficiency in intramolecular electron transfer, facilitating the conversion of protons into molecular hydrogen (H_2). The selection of bridging ligands, such as tetrapyrido [3,2-a:2',3'-c:2",3"'-j] phenazine (tpphz), plays a crucial role in directing electron flow toward the catalytic center, thereby enhancing efficiency. Comparisons with iridium (Ir) and osmium (Os) complexes suggest that Ru-based systems offer a superior balance of photostability, efficiency, and cost-effectiveness. Furthermore, theoretical calculations

indicate that strong π-acceptor ligands contribute to prolonged charge separation, which improves photocatalytic performance. (Putra et al., 2023)

The photochemical process begins when a molecule absorbs a photon, as shown in Equation 1. This energy absorption elevates an electron from the highest occupied molecular orbital (HOMO) to the lowest unoccupied molecular orbital (LUMO):

$$PS + hv \longrightarrow PS^* \qquad \text{(Eq.1)}$$

The excited molecule, now unstable, rapidly returns to its ground state by releasing the absorbed energy through various pathways, including radiative and non-radiative decay, as illustrated in Figure 1.1. These processes can be summarized as follows:

- Radiative decay: Return to the ground state with photon emission.
- Non-radiative decay: (i) Energy dissipation as heat, (ii) formation of products, (iii) quenching by another molecule (Q).

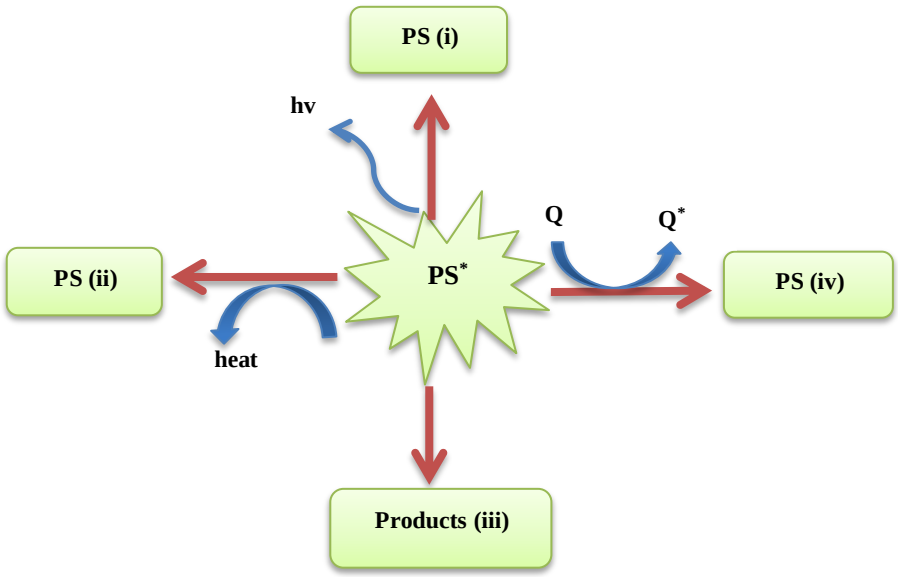

Figure 1.1: Deactivation of PS* by radiative and non- radiative. (Bushira,A., et al. (2024).

In transition metal complexes, radiative and non-radiative decay pathways compete. Unimolecular processes (i-iii) occur within a single molecule, while bimolecular processes (iv) involve interactions with another molecule.

1.2 Photo-Induced Excitation of Metal Complexes

Charge transfer (CT) is a fundamental phenomenon in photophysics and photochemistry. In CT transitions, electrons move between weakly associated donor (D) and acceptor (A) electronic states via radiative or non-radiative mechanisms (Balzani, 2001).

In metal complexes, CT occurs between the central metal atom and its surrounding ligands. These transitions are categorized into:

- Ligand-to-metal charge transfer (LMCT)
- Metal-to-ligand charge transfer (MLCT)

MLCT transitions are commonly observed in complexes containing low-lying π^* orbitals, such as aromatic ligands (bpy, CO, CN^-, SCN^-). The MLCT transition typically occurs at lower energy in the visible spectrum, particularly when the metal ion has a low oxidation state, such as Fe (II), Re(I), Ru (II), Ir (III), and Os (III) (Hei Yip & Wing Lo, 2018; Miessler et al., 2013).

The absorption band corresponding to intramolecular electronic CT is influenced by the ionization potential of the donor, the electron affinity of the acceptor, and the electrostatic attraction between them (Thauer et al., 1996).

D^6 transition metal complexes, including Fe (II), Ru (II), and Os (II), have attracted interest due to their electrochemical and photophysical properties. Ligand field theory describes these complexes as adopting an octahedral geometry, which may be distorted based on ligand interactions (Lombardi et al., 2001). (Insert Figure 1.2: Molecular orbitals of octahedral symmetrical complexes, adapted from Nicolet et al., 2002)

When comparing the transition metals in group 8 in their M^{+2} oxidation states, Fe (II) complexes are kinetically labile, meaning they undergo faster ligand substitution reactions, and their MLCT transitions occur at high energy. In contrast, Ru (II) complexes exhibit lower-energy MLCT transitions due to the presence of higher-energy metal-centered orbitals, facilitating longer-lived excited states. Os (II) complexes are kinetically inert, but they feature low-lying ligand-centered metal oxide semiconductors (MOs), which influence their MLCT behavior (Groß et al., 2016).

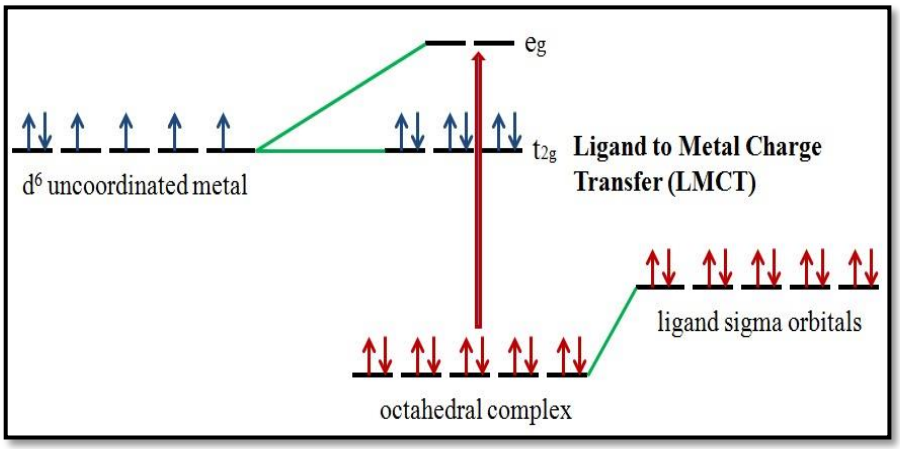

Figure 1.2: Represents the Mos of the Octahedral symmetrical complexes. The LMCT with π-donor ligand (Top) and MLCT with π-acceptor ligands (Bottom). (Nicolet et al., 2002).

Flash photolysis experiments reveal that $[Ru(bpy)_3]^{2+}$ absorbs light (~450 nm), exciting an electron from a metal-centered orbital to a π* orbital on the ligand, leading to an MLCT transition. This transition forms a singlet excited state, which undergoes intersystem crossing (ISC) to produce a long-lived triplet state, $^3[Ru(bpy)_3]^{2+*}$, capable of both oxidation and reduction reactions (Kalyanasundaram, 1982; Campagna et al., 2007).

1.3 Marcus Electron Transfer Theory and Its Application to Ru/Pt Complexes

The Marcus Electron Transfer Theory (MET) explains the transfer of electrons between donor and acceptor molecules in redox reactions. Developed by Rudolph Marcus, this theory provides a quantitative model for electron transfer rates based on reorganization energy and driving force (ΔG°).

The electron transfer rate (K_{ET}) is given by the following equation:

$$K_{ET} = A \exp \frac{-(\Delta G^\circ + \lambda)^2}{4\lambda k_B T}$$

Where:

- **A**: Electronic coupling constant (depends on orbital overlap).
- **ΔG°**: Free energy change of the reaction.
- **λ**: Reorganization energy (including solvent and nuclear reorganization).
- **$k_B T$**: Thermal energy at temperature T.

(Marcus, "Electron Transfer Reactions in Chemistry: Theory and Experiment," Nobel Lecture, 1993).

From a kinetic perspective, the CT or energy transfer (ET) rate depends on the excited-state lifetime. If the excited-state lifetime exceeds ~10^{-9} seconds, the excited donor (D*) has a greater chance of encountering the acceptor (A). During this interaction, specific weak interactions occur, leading to excited-state deactivation via second-order kinetic processes, as illustrated in Figure 1.3. (Ward, 1997; de Silva et al., 2000).

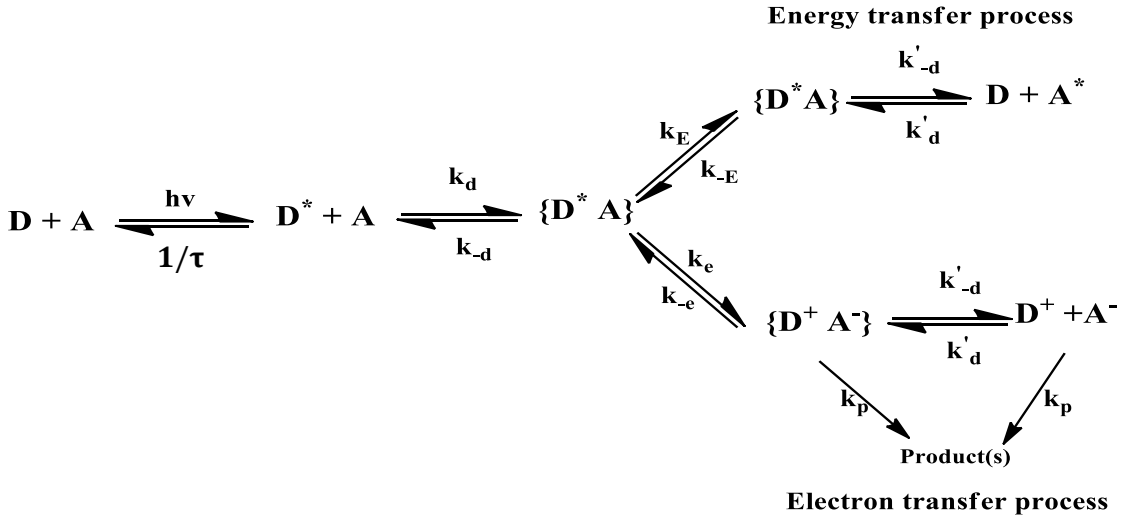

Figure 1.3: Representative kinetic mechanisms of electron transfer (ET) and charge transfer (CT) processes. Represents the diffusion rate constant of the donor and acceptor forming the complex D*A, which then undergoes charge transfer (CT) to form D^+A^- with a rate constant k_e. Finally, the dyad dissociates via the diffusion rate constant k'_{-d}. Since diffusion is the slowest step in this mechanism, the overall reaction is diffusion-controlled. (Ward, 1997).

The electron transfer rate involving excited-state molecules can be described using Marcu's theory. This transfer is thermally induced through geometric reorganization of surrounding molecules, as depicted in Figure 1.4. This process is known as the "outer-sphere" mechanism when it involves solvent reorganization and the "inner-sphere" mechanism when ligand rearrangement occurs within the molecule, forming favorable geometric structures before electron transfer. (Marcus, 1993; Marcus, 1989). In the Marcus model, solvent polarization significantly impacts the activation free energy of CT and, consequently, its rate.

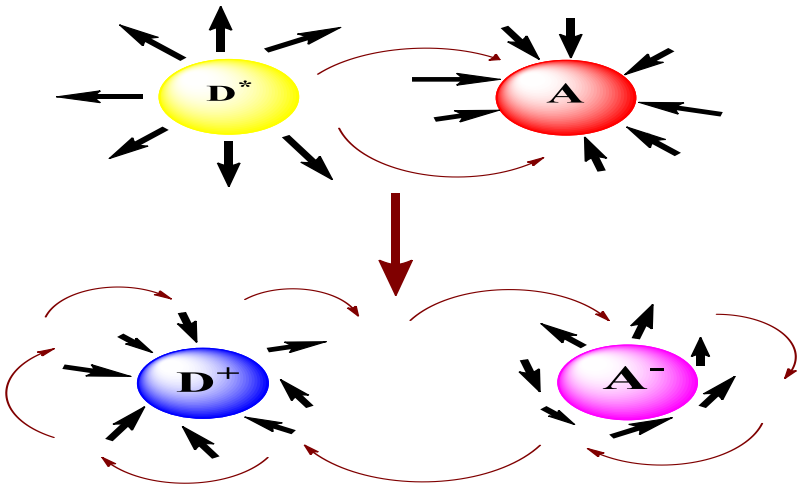

Figure 1.4: A schematic representation of solvent reorganization dynamics that facilitates electron transfer in a dyad based on the Marcus model system. (Marcus, 1993)

The initial and final states of electron transfer in excited molecules are represented as potential energy curves. The calculated free energy change (ΔG) involves the redox potential of the excited-state couple D*A. (Marcus, 1993) Another crucial pathway for excited-state energy dissipation is energy transfer, where both states remain locally excited but are localized in different molecular regions or separate molecules.

In ET, three mechanisms are proposed:

1. **Radiative Electron Transfer (ET)**, also known as trivial ET.
2. **Non-radiative Förster Resonance Energy Transfer (FRET)**, where ET is governed by electrostatic coupling of transition dipole moments, leading to donor (D) excited-state deactivation and acceptor (A) excitation. This mechanism operates over several nanometers and is orientation- and distance-dependent (inversely proportional to the sixth power of the distance).
3. **Non-radiative Dexter Energy Transfer**, also known as the exchange mechanism, which is a short-range process requiring orbital overlap between excited and ground electronic states. Here, a simultaneous opposite electron transfer occurs between the excited and ground states of the dyad.

The Dexter ET mechanism (Figure 1.5) dominates when the dyads are in direct contact and competes with the Förster mechanism for singlet excitation energy transfer.

However, it is significantly faster than Förster transfer in triplet excitation energy transfer is. (Mikhnenko et al., 2015)

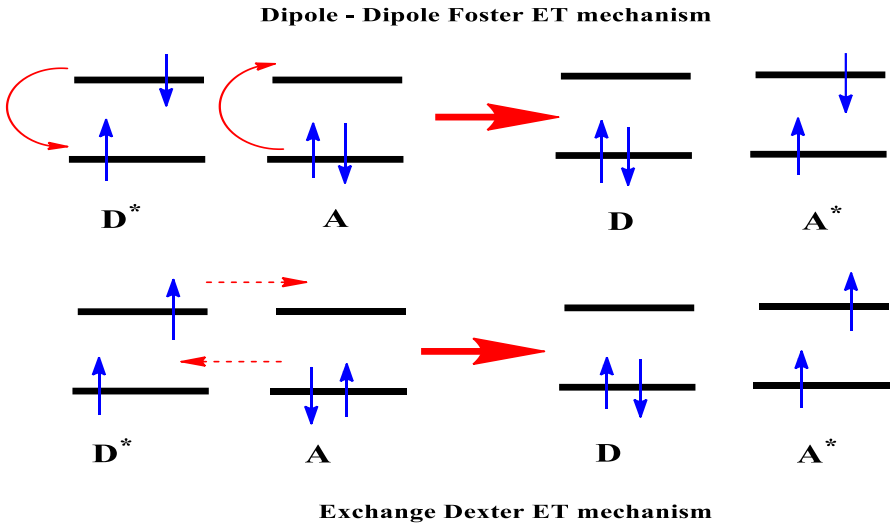

Figure 1.5: illustrating energy transfer dynamics based on the Förster mechanism (dipole-dipole) (top) and the Dexter mechanism (exchange) (bottom) (Mikhnenko et al., 2015).

1.4 Application of Marcus Theory to Ru/Pt Photocatalysts

In Ru (II)/Pt (II) complexes used for photocatalysis, electron transfer mechanisms play a critical role in reaction efficiency. Ru/Pt complexes function as photoactive catalytic systems where Ru (II) absorbs light to excite electrons, which are subsequently transferred through the tpphz bridging ligand to the Pt (II) catalytic center. Here, ions are reduced to molecular hydrogen (H_2), contributing to clean hydrogen fuel production as illustrated in Figure 1.6.

Marcus Theory explains this process through the following factors:

- **Role of Reorganization Energy (λ)**
  - Lower results in faster electron transfer.
  - π-Conjugated bridging ligands like tpphz reduce, improving electron transfer efficiency.
- **Effect of Solvent on Electron Transfer Rates**
  - In highly polar solvents (such as DMSO), the excited state is stabilized, modifying and thus influencing electron transfer rates.
  - This effect is evident in Ultraviolet - Visible (UV-Vis) spectra, where MLCT transitions appear at 435.02 nm in methanol, 448.24 nm in

acetonitrile, and 574.99 nm in DMSO, which will be discussed in Chapter 3.

- **Comparison of Different Ligands and Their Impact on Electron Transfer**
  - When chloride (Cl^-) is replaced by iodide (I^-), the wavelength shifts and interaction strength increases, leading to enhanced photocatalytic efficiency.
  - This explains why Ru/Pt-I_2 complexes exhibit higher catalytic activity compared to Ru/Pt-Cl_2 complexes. (Marcus, 1989)

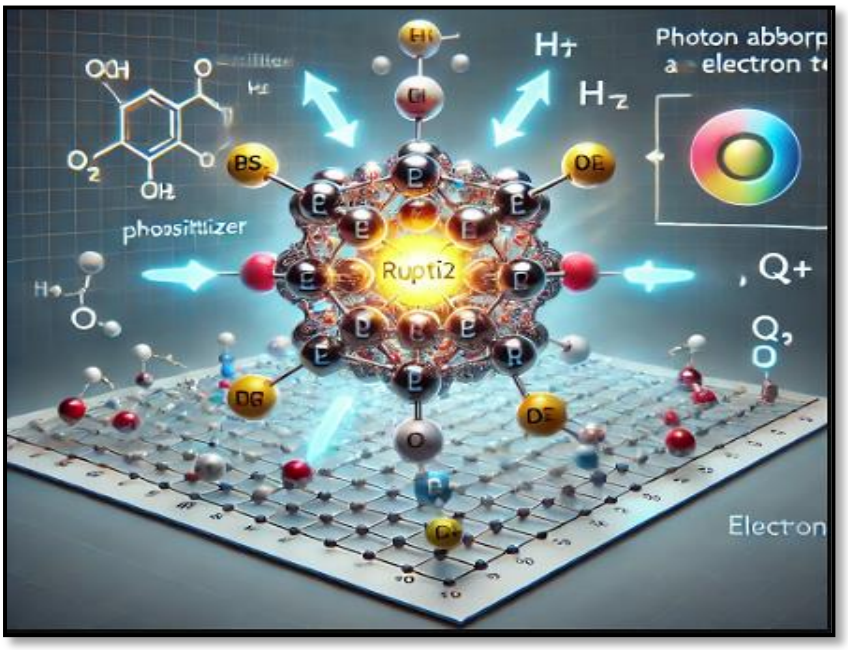

Figure 1.6: 3D Representation of the photodecomposition mechanism incorporating the Photoruptide PS*

1.5 Electronic Transition Calculation

The electronic transitions of ruthenium (II) complexes were investigated using time dependent density functional theory (TD-DFT) computations. The equation below defines the relationship between the electronic transition intensity and the oscillator strength (f_{OSC}):

$$f_{osc} = \int \varepsilon(\bar{v})d\bar{v} = \frac{4\pi^2 N_A \bar{v}}{3 \times 10^4 cn^2 \hbar l} \left|\vec{M}\right|^2$$

where f_{OSC} represents the oscillator strength, ε ($\bar{v}$) is the molar absorptivity, N_A is Avogadro's number, n is the refractive index of the solvent, ħ is Planck's constant, l is the path length, and $\overrightarrow{M}$ is the transition moment vector.

Accordingly, electronic transitions can be determined by computing the energies of active vertical transitions and their transition moments. Subsequently, the energy of the initial excited state was identified.

The energies of the first excited states of each Ru (II) complex were estimated, and the active electronic transitions were determined based on those with a nonzero f_{OSC} (active electronic transition; $f_{OSC} \neq 0$). As a result, the energy of the electronic transition between the excited and ground states, along with the corresponding wavelength, was calculated.

Based on quantum chemical calculations, a strong solvatochromic effect was predicted in a light-driven molecular photocatalyst for hydrogen generation. It was demonstrated that the electronic and optical properties of the photocatalyst strongly depend on the solvent in which it is dissolved. Specifically, the calculations indicate a solvent-dependent relocation of the HOMO orbital.

At high solvent dielectric constants, the HOMO is localized at the metal center of the photosensitizer, whereas at low dielectric constants, it is centered on the metal atom of the catalytically active complex. By elucidating the electronic origins of this strong solvatochromic effect, the implications of these findings for photocatalyst performance in different environments can be better understood. The table below presents the molecular orbital transitions of the Ru/PtI_2 complex in methanol (CH_3OH), acetonitrile (CH_3CN), and dimethyl sulfoxide (DMSO), detailing the electronic transitions, their corresponding energy levels, and oscillator strengths. (Putra, et al., 2023).

Table 1.1: Molecular Orbital Transitions of Ru/PtI_2 Complex in Different Solvents

Methanol

State	Transition	Orbital Transition	Contribution (%)	VEE (eV)	Wavelength (nm)	Oscillator Strength (f)
S1	286 → 287	d(Ru) → π*(tpphz)	89.59	2.1643	572.86	0.0005
S3	284 → 287	d(Ru) → π*(tpphz)	95.96	2.3224	533.86	0.0561
S13	284 → 290	d(Ru) → π*(tpphz)	62.88	2.7638	448.60	0.1809
	284 → 291	d(Ru) → π*(bpy)	26.82	-	-	-
S17	281 → 287	d(Pt),nI → π*(tpphz)	44.94	2.8501	435.02	0.2613
	284 → 291	d(Ru) → π*(bpy)	25.19	-	-	-

	285 → 292	d(Ru) → π*(bpy)	20.12	-	-	-
S20	284 → 292	d(Ru) → π*(bpy)	65.03	2.9055	426.73	0.1429
S33	281 → 289	d(Pt),nI → π*(tpphz)	77.66	3.1993	387.54	0.1395

Acetonitrile

State	Transition	Orbital Transition	Contribution (%)	VEE (eV)	Wavelength (nm)	Oscillator Strength (f)
S1	286 → 287	d(Ru) → π*(tpphz)	89.65	2.1618	573.51	0.0005
S3	284 → 287	d(Ru) → π*(tpphz)	95.92	2.3235	533.61	0.0562
S13	284 → 290	d(Ru) → π*(tpphz)	63.73	2.7660	448.24	0.1834
	284 → 291	d(Ru) → π*(bpy)	26.35	-	-	-
S17	281 → 287	d(Pt),nI → π*(tpphz)	26.74	2.8541	434.40	0.2625
S20	284 → 292	d(Ru) → π*(bpy)	64.85	2.9063	426.60	0.1441
S33	281 → 289	d(Pt),nI → π*(tpphz)	80.20	3.2061	386.72	0.1325

Dimethyl Sulfoxide

State	Transition	Orbital Transition	Contribution (%)	VEE (eV)	Wavelength (nm)	Oscillator Strength (f)
S1	286 → 287	d(Ru) → π*(tpphz)	90.02	2.1563	574.99	0.0005
S3	284 → 287	d(Ru) → π*(tpphz)	95.93	2.3170	535.11	0.0570
S12	284 → 290	d(Ru) → π*(tpphz)	66.10	2.7620	448.89	0.1923
S17	284 → 291	d(Ru) → π*(bpy)	43.32	2.8549	434.28	0.2207
S20	284 → 292	d(Ru) → π*(bpy)	65.61	2.9032	427.06	0.1478
S33	281 → 289	d(Pt),nI → π*(tpphz)	80.67	3.2209	384.94	0.1244

Table 1.1 presents the results of TD-DFT calculations for the molecular orbital transitions of the Ru/Pt I_2 complex in CH_3OH, CH_3CN, and DMSO. The estimated wavelengths of the electronic transitions in the MLCT region were 435.02 nm, 448.24 nm, and 574.99 nm, respectively. These calculated wavelengths show excellent agreement with the experimental values presented in Chapter 3. Such consistency between theoretical and experimental results confirms the reliability of the conducted computations.

1.6 Mechanism of Photocatalytic Hydrogen Generation Utilizing a Dinuclear Ru/Pt Complex

Dinuclear Ru/Pt the complexes represent a unique category of photocatalytic molecular components that depend on intramolecular charge transfer. As previously stated, intramolecular charge transfer refers to the movement of electrons induced by photons within a specific molecular assembly (Lämmle et al., 2022).

This assembly consists of three primary centers with varied photochemical characteristics and roles, as indicated in **Figure 1.7:**

Photosensitizer (PS) – a nucleus tasked with binding incident photons.

Catalytic center (Cat) – where catalytic reactions take place.

Bridging ligand (B) – the unit that connects the two functional centers.

Upon photon absorption, the photosensitizer undergoes an electronic transition to an excited state. The electron is subsequently moved to the bridging ligand, which must have a lower-energy π orbital to establish an energy a gradient, facilitating the spontaneous passage of electrons in the appropriate manner from the photosensitizer to the catalytic center. In the subsequent sections, we will examine the essential characteristics of all the
functional parts within this molecular assemblage. (Gedert et al., 2021).

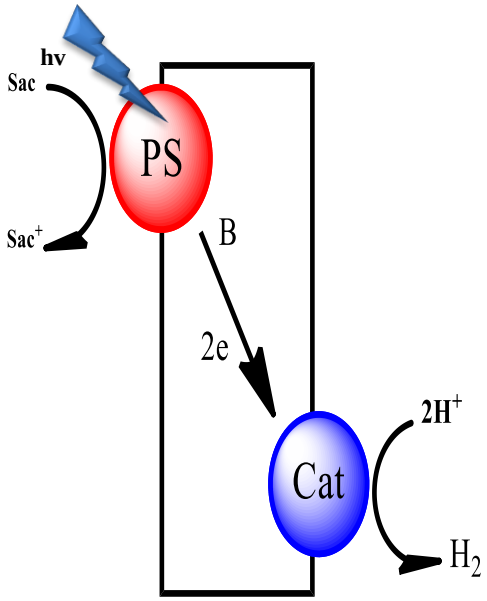

Figure 1.7: Intramolecular Approach (Gedert et al., 2021)

1.7 Vectorial Electron Transfer in Ru/Pt Complexes

The vectorial electron transfer process occurring in Ru/Pt complexes upon irradiation can be summarized as follows:

Efficient vectorial electron transfer is essential for this molecular assemblage to successfully generate hydrogen. The process initiates with light absorption at the ruthenium center, subsequently leading to electron transfer via the bridging ligand to the platinum moiety, which functions as the catalytic center. This leads to the oxidation of the Ru (III) center, which reverts to its ground state following electron transfer to the bridging portion.

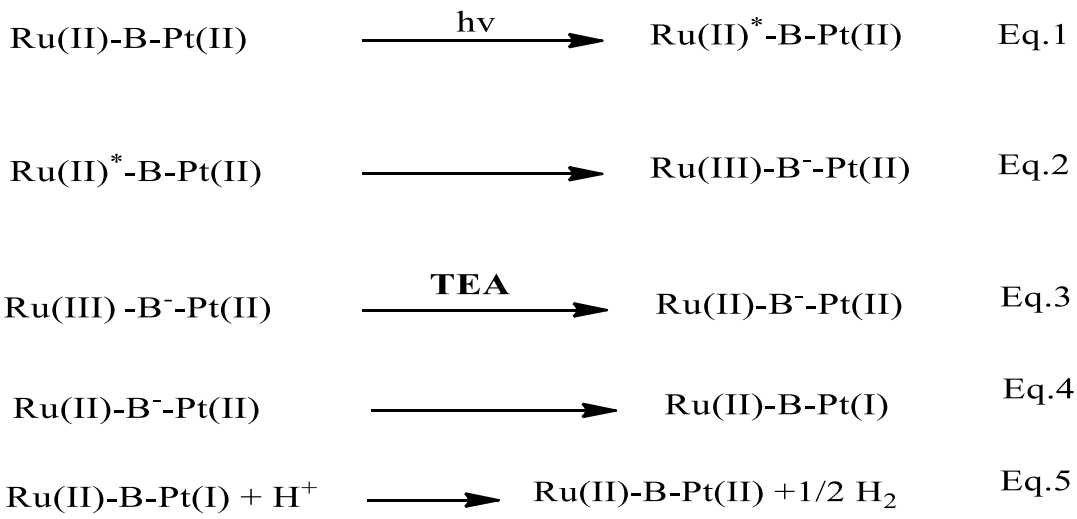

Scheme 1.1a: Photocatalytic Assembly Reaction and Hydrogen Production

A sacrificial reductant, triethylamine (TEA), is necessary to decrease the oxidized Ru (III) atom at the light absorbing core, thus enabling the subsequent photoexcitation cycle to initiate. Nonetheless, the utilization of sacrificial agents such as TEA can pose challenges, since they may disrupt the photocatalytic process.

The subsequent scheme demonstrates that TEA decomposes following the initial electron transfer, resulting in the generation of protons and electrons via non-photonic reactions. Two protons and one electron are produced during this process. As noted earlier, these reactive species may lead to the degradation of the photocatalytic molecule. (Lämmle et al., 2022).

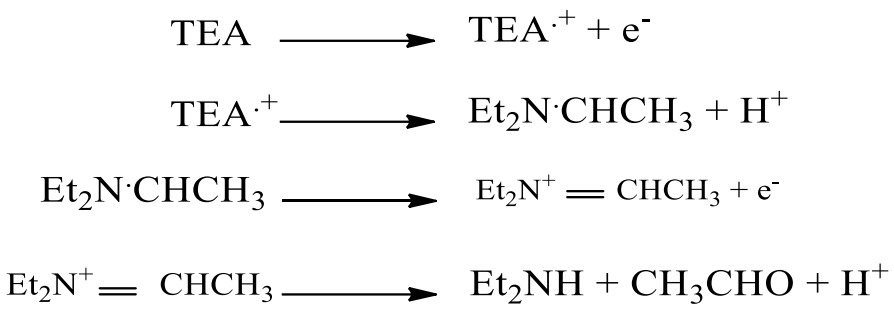

Scheme 1.1b: TEA Decomposition

1.8 Photocatalysis

Photocatalysis plays a crucial role in environmental remediation and renewable energy technologies. The ability to objectively characterize photocatalyst properties and photocatalytic processes is essential for accurate performance evaluation and fundamental research, which guide the design and development of high-performance photocatalysts and photocatalytic systems.

Photocatalysis is fundamentally an electron transfer mechanism in which energy is directed to a catalytic center, which then utilizes this energy to drive photocatalytic reactions, ultimately generating hydrogen gas from water. Figure 1.8 illustrates that any photocatalytic molecular system intended for hydrogen production must include four essential components.

1. An active region for photoredox reactions; it can absorb electromagnetic radiation from sunlight and act as a photosensitizer.
2. A catalytic center facilitates the reduction of protons to generate gaseous hydrogen.
3. An electron transfer linker facilitates the transfer of electrons from the photoactive center to the catalytic center.
4. A sacrificial electron donor is present in excess to provide electrons for the regeneration of the photosensitizer. (Liu et al., 2023)

1.8.1 The Significance of Peripheral Ligands in Photocatalytic Assembly

Peripheral ligands play a crucial role in the photosensitizer center of that photocatalytic assemblage, as they coordinate the metal center exhibiting higher photocatalytic activity. The electronic properties of these ligands and the characteristics of the metal

influence the energy of the excited state and the absorption wavelength. Ligands must be engineered to occupy the upper range of the energy gradient to promote vectorial electron transfer from the harvesting of light unit to the catalytic center through the bridging ligand, which is chosen to be positioned at the lower end of the energy gradient. The electronic coupling between the peripheral ligands and the bridging ligand must be optimized to facilitate electron transfer from the peripheral ligands onto the bridging ligand, preventing the excited state of the peripheral ligands from decaying to the ground state with no electron transfer. This elucidates the reason that compounds facilitating direct population of ^{3}MLCT states within the bridging ligand demonstrate enhanced photocatalytic ability.

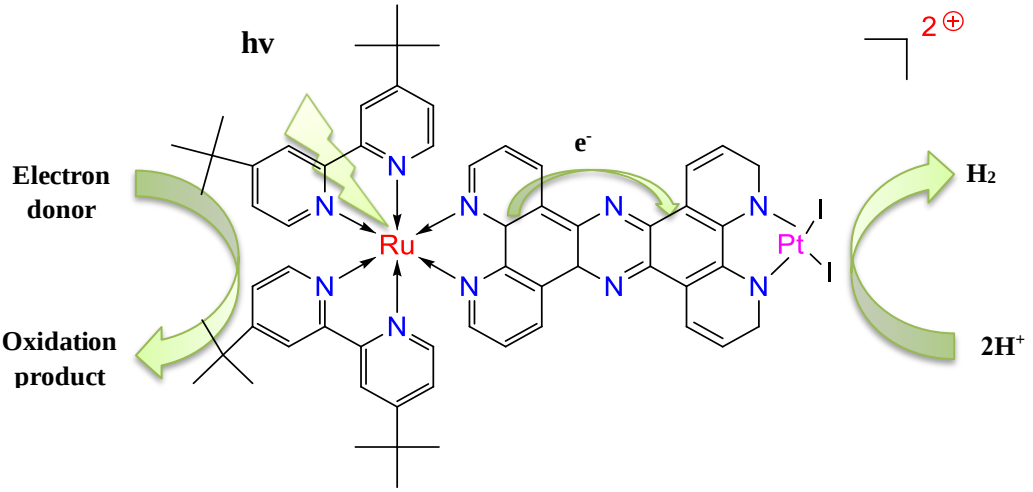

Figure 1.8: Mechanism of Photocatalytic Hydrogen Generation Utilizing [Ru(L)$_2$tpphz] $^{2+}$. (Rau et al., 2006)

Compounds **(1), (2**) as illustrated in Figure 1.9, serve as examples. The absorption characteristics of the two peripheral ligands exhibits similarity. Compound **(1)** includes bpy, a common component, while compound **(2)** features two ester groups linked to the peripheral ligand. Although the two ligands appear similar, they demonstrate markedly distinct photocatalytic behaviors. In both instances, the bridge includes a pyrazine unit, which exhibits the lowest MLCT state, likely attributable to the bridging ligand at approximately 530 nm.

Compound **(1)** demonstrates an absence of photocatalytic activity as there is not observed hydrogen evolution. Introducing a group of esters to the peripheral ligands in compound **(2)** led to a turnover number (TON) of 400 after 18 hours of irradiation. This

indicates that esterification improves the π-acceptor characteristics of the peripheral ligands, resulting in a reduction of their π* energy levels and an enhancement of electronic coupling with the bridging ligand. (Schulz et al., 2011).

1.8.2 The Significance of a Bridging Ligand in Photocatalytic Assemble

The bridging ligand serves as a covalent and electrical connection among the photosensitizer center and the supramolecular catalytic entity, employing the conjugated π-electron system. It coordinates with both the metal in the photosensitizer center and the metal in the catalytic center, necessitating two bidentate coordination sites at each terminus. The interaction among the photocatalytic supramolecular assembly units is significantly affected by the dimensions, morphology, and electronic characteristics of the bridge.

The bridging ligand is developed with multiple essential factors in consideration. It should be adequately lengthy to facilitate unidirectional photoinduced electron transfer while reducing reverse electron transfer. The molecular design must ensure that the ^{3}MLCT state is localized on the bridging ligand instead of the peripheral ligands.

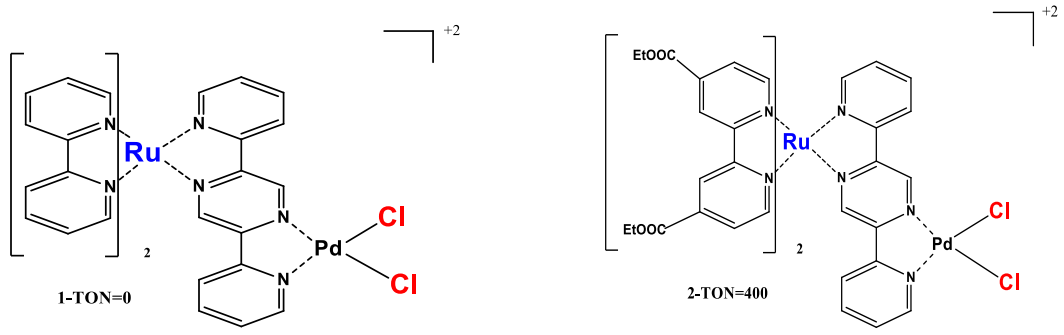

Figure 1.9: Photocatalyst structure (1,2). (Halpin et al., 2013)

Figure 1.10 presents experiments that demonstrate the impact of the bridging ligand. Compounds **(3), (4)** are noteworthy, as they are identical in all respects except for the bridging ligand. 430 TON of hydrogen generated from **(3)** following eighteen hours of irradiation, while **(4)** exhibited no activity. The observed difference is attributed to the localization of the lowest unoccupied molecular orbital (LUMO). Resonance Raman spectroscopy and DFT (density functional theory) computations indicate that in **(3)**, the orbital is localized on the bridging ligand, while in **(4)**, it is primarily localized on the

bpy ligands and the Ru center. This configuration hinders effective electron transfer from the harvesting of light unit to the catalytic center. (Bindra et al., 2012).

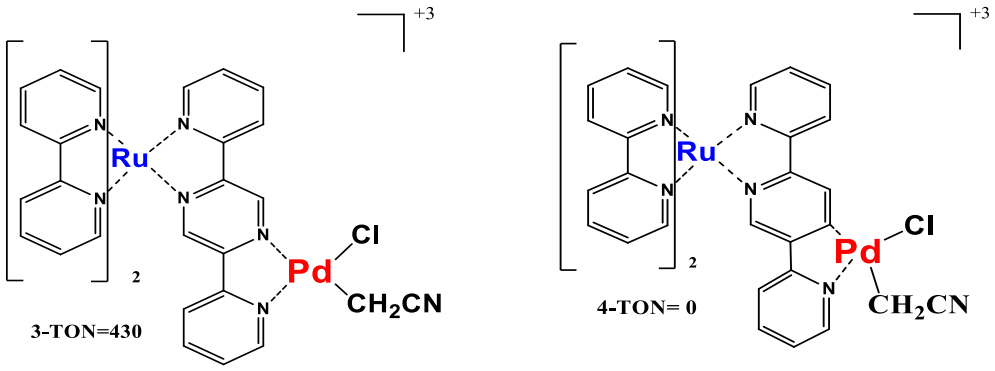

Figure 1.10: Photocatalyst structure (3,4). (Halpin et al., 2013)

Rau et al. performed minor chemical modifications to the bridging ligand, as illustrated in Figure 1.11, and evaluated the catalytic activity of Ru/Pd complexes. For example, the incorporation of bromide into the tetrapyrido phenazine bridging moiety of complex **(1)** resulted in complex **(8)**, which exhibited a notable decrease in catalytic activity to 69 TON after eighteen hours, in contrast to 210 TON for the parent complex **(1)**.

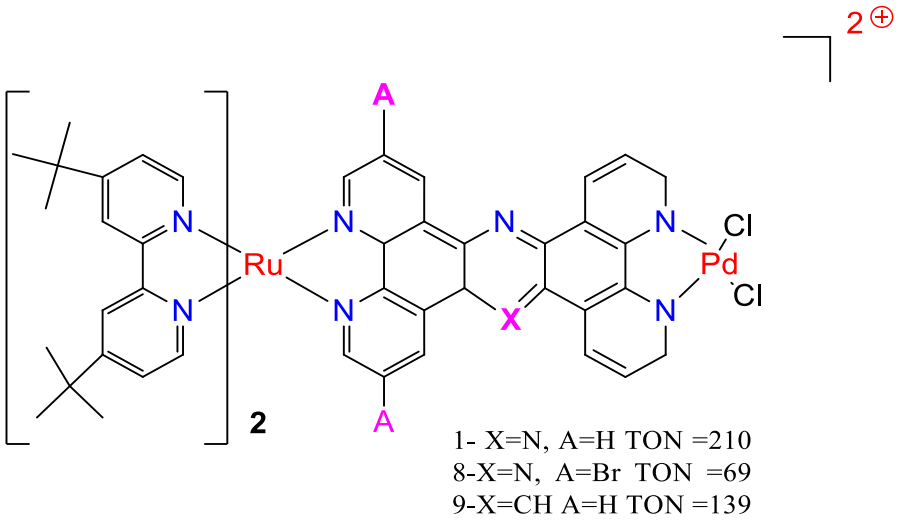

Figure 1.11: Photocatalyst Configuration of complexes 1, 8, and 9.

In **(9)**, substituting a pyrazine ring of tpphz with an acridine component yielded a catalytic activity of 139 TON, in contrast to the 210 TON recorded for the parent **(1).**

These findings highlight the essential function of the bridging ligand in the development of efficient photocatalytic assemblies. (Karnahl et al., 2011; Karnahl et al., 2012).

1.8.3 The Effect of Wavelength

As previously mentioned, during the photoexcitation of compound 1, the initial photo-induced excited state resides in the peripheral ligands. Furthermore, the distribution about the bridging ligand is critical for catalytic activity, as it allows photoinduced electron transport to a catalytic site. The disparities into excited state energies between the peripheral and bridging ligands are essential for establishing an energy gradient that facilitates swift electron transfer in the appropriate direction. Moreover, the intensity of their electronic coupling constitutes a significant factor. In this context, NH_2PF_2 is the most suitable substance for these studies.

As an example, compounds **2 and 3**, shown in Figure 1.12, exhibits very similar absorption characteristics. In both cases, the bridge contains pyrazine unit, which has the lowest MLCT states, due to the influence of the bridging ligand. (Champness, 2011)

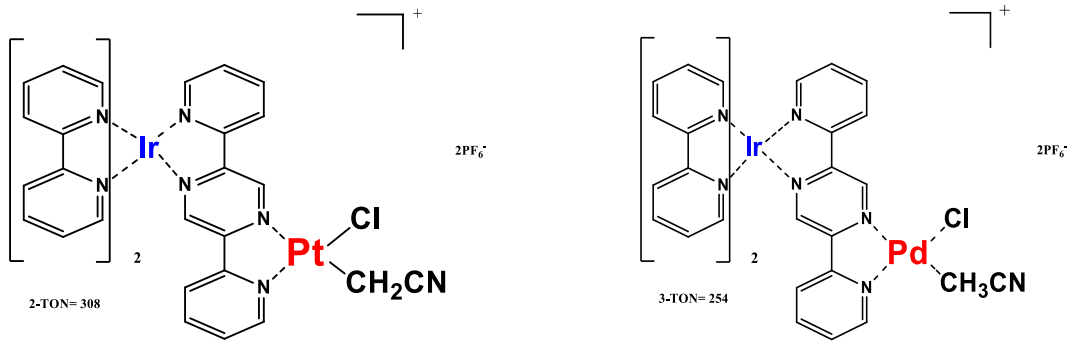

Figure 1.12: Photocatalyst Configuration of 2,3. (Halpin et al., 2013; Soman et al., 2012)

Upon illumination around 470 nm, the compounds yield (TON) values of 308 and 254, respectively, signifying a disparity in photocatalytic performance. Upon irradiation of both complexes at 350 nm, the (TON) values diminish to 65 and 16 for **(2,3)**, respectively. This discovery unequivocally illustrates that the type of illumination profoundly influences the photocatalytic efficacy of these complexes.

Bernhard and his colleagues have conducted extensive studies on the intermolecular excitation transfer mechanism in Ir (III) complexes, revealing that compounds **2 and 3**

exhibit high stability as photosensitizers. This enhanced photostability has been observed in various iridium complexes that function as photocatalysts for hydrogen photogeneration via an intermolecular excitation transfer mechanism. (Goldsmith et al., 2005; Zanoni et al., 2014)

The stability observed is due to the higher ligand field stabilization the power of third row elements, providing Ir (III) complexes a notable advantage over ruthenium (III) complexes, as evidenced by the comparison of compounds 2 and 3. It is important to note that ruthenium (II) serves as the primary reference material in these studies. In the case of second row elements, direct individuals of the triplet metal centered excited state can lead to ligand dissociation and subsequent decomposition, a process not seen in Ir (III)-based analogs. (Watts & Houten, 1974)

1.8.4 The Effect of Photocatalytic Type on the Stability of Ru/Pt for Solar-Driven Hydrogen Generation

Molecular photocatalysts for hydrogen production that mimic natural photosynthesis have been extensively studied in recent years (Blanchette, 2008). Since the first reports on H_2-evolving Ru/M (M = Pt or Pd) bimetallic photocatalysts were independently published, significant efforts have been made to improve H_2 generation efficiency in terms of both the TON and turnover frequency (TOF). Optimizing photocatalytic efficiency is challenging due to the complex nature of photophysical and photochemical processes that occur across multiple timescales. A sacrificial agent, such as TEA, is required to regenerate the photosensitizer by donating electrons to the formally oxidized Ru (III) center (Schulz et al., 2012; Banerjee et al., 2017).

The hydrogen (H_2) economy is expected to play a crucial role in addressing global challenges such as anthropogenic climate change and rising energy demands. Developing the H_2 economy requires clean, cost-effective, and sustainable methods for producing H_2 from renewable energy sources. A promising approach for localized H_2 production is the direct conversion of solar energy into fuel. Intramolecular photocatalytic systems, which include a light-harvesting unit, a bridging ligand, and a catalytic center, offer significant opportunities (Schulz et al., 2022).

Several bimetallic systems have been reported, using combinations such as Ru-Re, Re-Co, Ru-Pt, Os-Rh, Ru-Rh, Pt-Co, and Ir-Rh. Systems where Ru (II)-based photosensitizers are covalently bound to Pt (II) or Pd (II) catalysts have received substantial attention. Platinum complexes, both mononuclear and homodinuclear, have been shown to act as catalysts for H_2 production (Inagaki & Akita, 2010). Rau et al. performed comprehensive studies on the photophysical properties of the following the complexes:

1. $[(bpy)_2Ru\ (2,3dpp)]^{2+}$ **[A-1]**
2. $[(bpy)_2Ru\ (2,3dpp)\ PtCl_2]^{2+}$ **[A-2]**
3. $[(bpy)_2Ru\ (2,3dpp)\ PtI_2]^{+2}$ **[A-3]** (Halpin Y et al., 2013)

All of the complexes **[A-1]**, **[A-2]**, and **[A-3]** were analyzed utilizing high-performance liquid chromatography (HPLC), UV/Vis absorption spectroscopy, and proton nuclear magnetic resonance (^{1}H-NMR). The HPLC data indicate that all compounds exhibit a singular dominant peak; however, the HPLC results for the dinuclear compounds revealed variations in retention duration, potentially attributable to the existence of catalytic states and the characteristics of the halogenated peripheral species. (Figure 1.13 illustrates the difference in halogen)

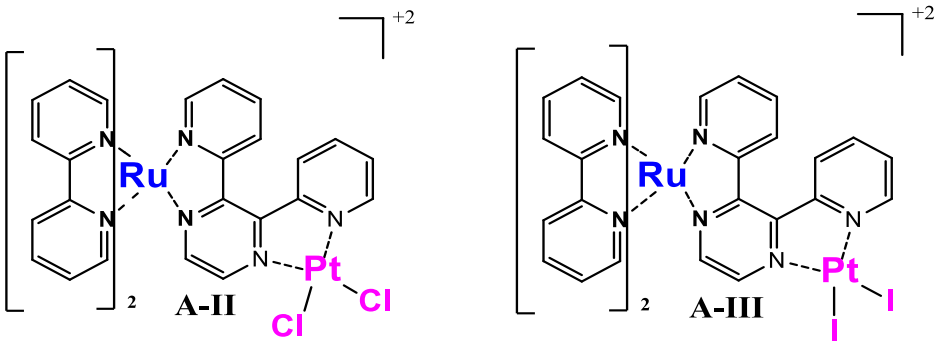

Figure 1.13: Structure of the A-2 and A-3 complexes.

The findings demonstrate that, upon radiation, the monomer exhibits photoreactivity, the dinuclear $Ru/PtCl_2$ center maintains photostability, and dinuclear Ru/PtI_2 center shows photoreactivity, albeit at a reduced frequency compared to the monomer, as illustrated in Figure 1.14(a).

The chromatograms show that the metal complexes decompose rapidly in the presence of (TEA) during irradiation. Notably, **[A-3]** species appear to decompose the fastest in

this setting. Based on the results of this study, it can be concluded that TEA is a highly reactive reagent that decomposes ruthenium complexes and acts as an electron donor in the presence of light, as shown in Figure 1.14(b) (Pfeffer M., et al., 2022)

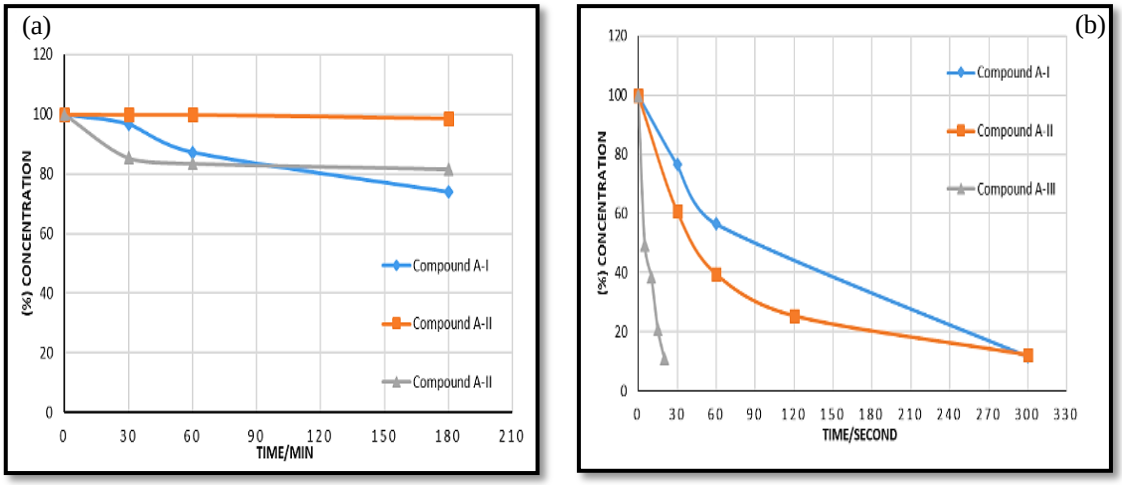

Figure 1.14: The photodegradation rates for compounds A-1, A-2, and A-3 are examined (a) without TEA and (b) with TEA. (Note: When A-1=A-I) (Pfeffer M., et al., 2022).

The chromatograms indicate that the metal complexes undergo rapid decomposition in the presence of TEA during radiation. Significantly, the A-3 species exhibit the highest rate of decomposition in this context. The findings of this investigation suggest that TEA is a highly reactive agent that decomposes Ru complexes and functions as an electron donor in the presence of light, as illustrated in Figure 1.14(b). (Pfeffer M., et al., 2022).

1.9 Objectives of the study

This study seeks to establish sophisticated analytical methods, including HPLC and UV-Vis spectroscopy, as efficient instruments for analyzing, characterizing, and assessing the stability of diverse photocatalytic chemicals pre- and post-illumination. The study investigates the influence of light exposure on the stability of photocatalytic compounds and using these methods to assess probable chemical alterations resulting from radiation contact.

The study will assess the stability of photocatalytic compounds based on ruthenium/platinum (Ru/Pt) intermolecular complexes with multidentate (N^N) chelating ligands. The influence of peripheral ligand at the ruthenium (II) center, such as 4,4'-tert-butyl-2,2'-bipyridine (Tbbpy), on the general behavior of the compounds

will be explored, particularly focusing on its role in the photocatalytic hydrogen evolution process (PHE). The influence of bridging ligand, Tpphz, will also be studied, as shown in Figure 1.15(b).

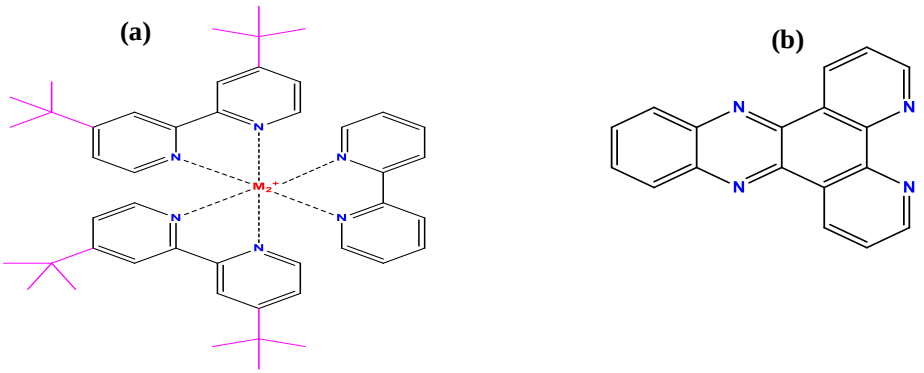

Figure 1.15: (a) Structure of the peripheral ligand Tbbpy. (b) structure of the bridging ligand Tpphz

This study will involve comparing compounds that contain platinum catalytic centers with those that do not, specifically investigating the impact of terminal ligands such as iodide and chloride regarding the catalytic activity of the compound. The comparison will provide deeper insight into the effect of substituting the influence of terminal ligands on the photocatalytic effectiveness and stability for these compounds.

This research will contribute new insights into the stability of photocatalytic compounds and strategies for enhancing their performance in renewable energy applications. By evaluating chemical changes and comparing various compounds, valuable data will be obtained that can be used to improve the design of photocatalysts for clean energy technologies.

CHAPTER 2

Experimental Part

2.1 Analysis of complexes

2.1.1 High Performance Liquid Chromatography

High Performance Liquid Chromatography, commonly referred to as High-Pressure Liquid Chromatography, stands as a leading and sophisticated chromatographic separation technique. It is routinely employed to effectively separate the components of a mixture, such as herbal extracts or products, identify each component to the greatest extent possible, quantify the separated components, and generate the chemical profile or fingerprint of a crude mixture (Mukherjee, 2015).

Chromatography is a mass transfer process characterized by adsorption, utilizing a nonpolar stationary phase and a polar mobile phase that traverses the column. The column's active component, the sorbent or stationary phase, is generally a granular material composed of solid particles (e.g., silica, polymers), typically measuring between 2 and 50 micrometers. The constituents of the sample mixture are separated based on their interactions with the sorbent particles, which are contingent upon their relative polarity. The pressurized liquid, or mobile phase, is usually a solvent mixture (e.g., water, acetonitrile, and/or methanol). Its composition and temperature significantly influence the separation process by affecting the interactions between the sample components and the sorbent. These interactions are physical, encompassing hydrophobic, dipole-dipole, or ionic forces (Snyder et al., 1979; Lindsay, 1992).

In the late 1980s, Valenty and Behnken used HPLC to monitor the reactions of tris(2,2'-bipyridyl) Ru, $[Ru(bpy)_3]^{2+}$ utilizing optical absorption at 280 nm as the detection parameter. This method's high sensitivity and ability to separate species with very similar structures made it possible to identify the products formed during the photochemical reaction of a complex of the kind $[Ru(bpy)_2(X)]^{n+}$ about a possible ten years later. (Buchanan et al., 1988; Buchanan et al., 1991; Bo Yin et al., 2004).

2.1.2 Exchange of Ions

Ion-exchange chromatography (IEC) segregates molecules based on their molecular charge or, for larger polymers and biomolecules, predominantly by their surface charge. Analyses with a charge contrary to that of the ion-exchange resin are maintained to differing extents. As the pH increases, the molecules gain a negative charge and attach

to an anion exchanger. Salt and pH gradients are employed to elute the compounds from the column. The pH of the eluent affects resolution by influencing the selectivity and ionic strength of the buffer, hence impacting retention.

- **Weak** resins
- **Strong** resins
- **Anion** resins (negative charge)
- **Cation** resins (positive charge)

Anion-exchange resins are synthesized by incorporating cations into the resin matrix, where the bound ions associate with mobile negatively charged counter-ions that can be exchanged with other ions present in the sample. Analyses exhibiting a greater affinity for the resin matrix than the counter-ions will be substituted. The ionic charge of the analytes is significantly influenced by pH (Fuquay, 2011).

2.1.3 Strong and Weak Ion Exchangers

Strong ion exchangers are generally composed of sulfonic and quaternary ammonium groups, whereas weak ion exchangers consist of several different functional groups. The labels "strong" and "weak" explicitly denote ionization behavior across a broad pH spectrum, rather than binding strength. The bonded phase is formed via covalent bonds between hydrocarbon groups and micro silica particles. When the hydrocarbon includes polar groups, the bonded phase exhibits normal-phase chromatographic characteristics, whereas, in the absence of these groups, it demonstrates reversed-phase chromatographic characteristics. Table 2.1 presents examples of functional groups commonly used in ion exchangers. If the hydrocarbon groups have an inorganic component, or if one is chemically added during future procedures, the bonded phase can serve as an ion exchanger. Various methods exist for the chemical attachment of groups to silica. Compared to polystyrene-based packings, ion-exchange packings with silica supports offer substantial benefits, such as increased selectivity and reduced column degradation. Resins with a glass or silica core exhibit superior structural integrity, minimizing issues such as swelling and bed settling. Furthermore, changes in buffer salts or the use of mixed solvents typically do not compromise column efficiency due to particle swelling. Bonded resin packings exhibit high thermal stability, withstanding temperatures of up to 80°C. However, extremely acidic (pH < 2) or slightly basic (pH > 8) conditions may compromise the integrity of the silica supporting

the bonded phases, resulting in diminished-column performance. (Lindsay,1992; Wellings, 2006; Show & Chattopadhyay, 2016)

Table 2.1: Functional Groups and Their Applications in IEC

Ion Exchanger Type	Functional Group	Strength	p Ka Value	Ionized State at Specific pH	Applications
Anion Exchangers	Quaternary Ammonium	Strong	<1	$-NR_3^+$ (Ionized)	Effective for separating phenolic compounds and carboxylic acids, especially in basic environments.
	Diethyl Aminoethyl	Weak	8	$-NHR_2^+$ (Ionized)	Suitable for weak anion separations, especially organic acids.
	Diethyl Aminopropyl	Weak	8	$-NHR_2^+$ (Ionized)	Suitable for separation of phenols and organic acids, offering moderate strength.
Cation Exchangers	Sulfo Propyl	Strong	<1	$-SO_3^-$ (Ionized)	Used for extracting and analyzing acidic analytes such as anthocyanins and alkaloids.
	Methyl Sulfonate	Strong	<1	$-SO_3^-$ (Ionized)	Effective for the removal of cations, especially in acidic conditions.
	Carboxymethyl	Weak	5	$-CO_2^-$ (Ionized)	Used for analysis of alkaloids and carboxylic acids, ideal in neutral conditions.

Strong ion exchangers are typically formed with sulfonic and quaternary amino groups, while weak ion exchangers are formed with a variety of other functional groups. Both "weak" and "strong" involve ionization behavior over a wide pH range, rather than bind strength.

Forceful ion exchangers maintain complete ionization across an extensive pH spectrum, while the dissociation and exchange capacity of weak ion exchangers fluctuate more markedly with pH variations. The principal attributes of strong ion exchangers encompass:

1. The sample loading capacity remains constant despite fluctuations in pH, as charge loss from the ion exchanger is minimal.
2. The interaction between the ion exchanger and the solute is straightforward, with a simple mechanism of action. (Gupta & Biswas, 2023)

2.1.4 Reversed-Phase HPLC Separation

The optimization of reversed-phase HPLC separation for ionizable organic molecules is a complex challenge. The retention of these components depends on multiple factors, including the type and composition of the eluent, the nature of the stationary phase, the presence of accessible residual silanols, as eluent pH, buffer type, and concentration. Secondary equilibria in the HPLC system also significantly affect analyte retention. (Twitchett & Moffat, 1975 ;Nagy, 1988 ;Cheong & Carr, 1990 ;Valkó et al., 1993 ;McCalley, 1996; Dolan, 2002) .

The retention of fully protonated analytes increases with the concentration of inorganic additives. The inclusion of salts, such as perchlorate, trifluoroacetate, and phosphate, enhances retention of completely protonated analytes while maintaining a constant pH of the mobile phase. This effect is attributed to the interaction between protonated analytes and the counter-anion of the acid or salt, which disrupts the analyte's solvation shell, leading to increased hydrophobicity and improved retention. (LoBrutto et al., 2001)

2.1.5 Ion Displacers in IEC

Ion displacers play a significant role in ion exchange chromatography, which are used to displace weaker ions from the stationary phase or elution phase. These displacers are carefully selected based on their ability to interact with specific ions and their strength in displacing them. The effectiveness of these displacers depends on their relative strength, with some displacers being more efficient in displacing strongly bound ions compared to others. They are essential for achieving efficient separations and ensuring that the desired analytes are isolated with high precision. The table below provides a detailed summary of the various ion displacers used in ion exchange chromatography, their strength, and their specific applications shown in Table 2.2.

These displacers can be strategically employed depending on the type of ion exchange required, whether for analytical separations, buffering, or in complex separation procedures. The strength of the displacer influences its ability to replace ions from the stationary phase, thus affecting the overall efficiency and selectivity of the chromatographic process. (Gupta & Biswas, 2023)

Table 2.2: Ion Displacers and Their Applications in IEC

Ion Displacer	Application in Ion Exchange Chromatography	Displacer Strength (Weak to Strong)
F^-	Suitable for displacing weaker anions in ion exchange processes.	Weak
OH^-	Used in the displacement of weakly retained anions and for pH adjustments.	Weak
CH_3COO^-	Effective for replacing anions like chloride in mild ion exchange conditions.	Moderate
Cl^-	Commonly used for displacing less strongly bound anions.	Moderate
SCN^-	Efficient in displacing strongly bound anions such as sulfate.	Strong
Br^-	Often used to replace weaker anions in ion exchange systems.	Strong
NO_3^-	Frequently used in ion exchange columns, particularly in buffering systems.	Strong
I^-	A strong displacer for a wide range of ion exchange applications.	Strong
$C_2O_4^{2-}$	Highly effective in displacing bound anions, particularly in complex separations.	Strong
SO_3^{2-}	Most effective for ion exchange of sulfate and other high charge density anions.	Very Strong
$C_6H_5O_7^{3-}$	Used in highly selective separations of anions with high affinities.	Very Strong

2.2 pH Effects and Buffer Types

IEC entails the exchange of ions between the counter ion of a charged functional group affixed to an insoluble resin matrix and a charged molecule possessing the same charge as the counter ion. The significance of pH and pKa in sustaining equilibrium is evident, along with the resin's ability to "capture" or bind the target analyte. Moreover, altering the charge and charge intensity on the resin facilitates the selective extraction of charged molecules from intricate matrices, such as those present in plant, animal, or food systems. Schematic diagram 2.1 provides a lucid representation of the theory of IEC and its associated equilibria. An essential feature of IEC is the capacity to modify a molecule's polarity by merely altering the pH, utilizing concepts similar to liquid/liquid partitioning, although without requiring emulsions. Since IEC basically depends on acid/base chemistry, the notions of pH and pKa offer a solid framework for comprehending ionization behavior, providing a more quantitative perspective. Thus, the pH of the mobile phase is crucial for facilitating chemical separation processes. (Dragull and Beck, 2012)

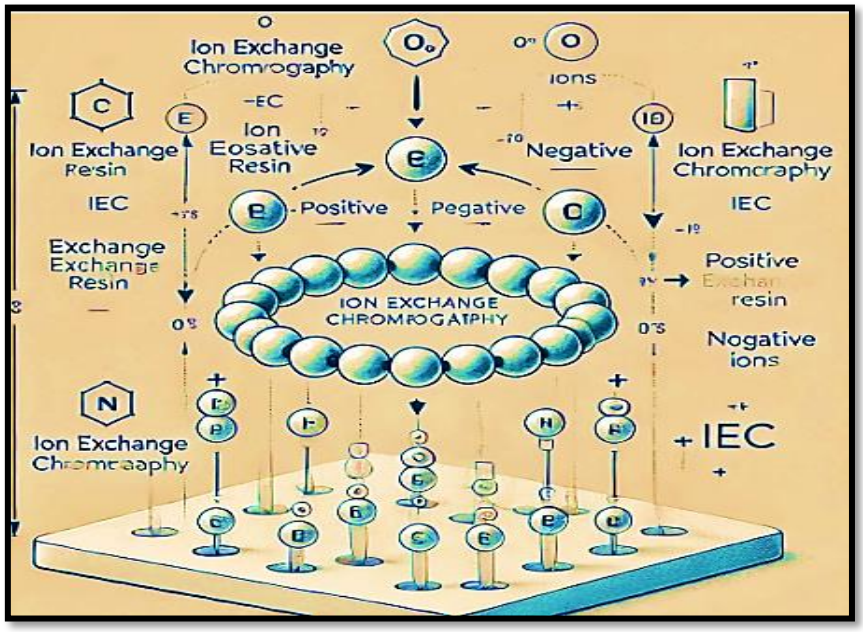

Schematic Diagram 2.1: The representation of IEC theory (Dragull and Beck, 2012)

The development and optimization of reversed-phase HPLC separation procedures for mixtures of ionizable organic molecules pose significant challenges. The retention of these ionizable components is influenced by various factors, including eluent type and composition, stationary phase characteristics, the presence of accessible residual silanols, eluent pH, buffer type, and concentration. Furthermore, secondary equilibria within the HPLC system can substantially impact analyte retention (Twitchett & Moffat, 1975 ;Nagy, 1988 ;Cheong & Carr, 1990 ;Valkó et al., 1993 ;McCalley, 1996; Dolan, 2002) .

Retention of fully protonated analytes increases as the concentration of inorganic additives rises. The addition of salts such as perchlorate, trifluoroacetate, and phosphate enhances the retention of protonated analytes while maintaining a constant mobile phase pH. This effect is attributed to the interaction between protonated analytes and the counter-anion from the acid or salt, which disrupts the solvation shell of the analytes, thus increasing their hydrophobicity and retention (LoBrutto et al., 2001).

2.3 Ionic Strength

Salts such as NaCl or Na_2SO_4 can increase the ionic strength of aqueous samples, reducing analyte solubility. Salt ions attract water, reducing the availability of analytes in solution and perhaps improving recovery. The effects of salt content should always be investigated experimentally.

2.4 Temperature and Time

Temperature significantly influences solid-phase extraction (SPE). Increasing the temperature accelerates the diffusion rate, reduces the equilibration time, and increases the analyte concentration in the headspace. However, higher temperatures may lead to reduced extraction efficiency as the distribution of the analyte between the stationary phase and the sample becomes less favorable. Conversely, lower temperatures result in longer equilibration times and slower diffusion (Zhang et al., 2017).

An essential component of extraction efficiency is equilibration time. Equilibration time is correlated with both flow rate and column size. Columns are usually flushed with enough volumes to guarantee proper equilibration, which necessitates meticulous flow rate control. The maximum detection limits are obtained at the ideal equilibration time. Early in the extraction process is when extraction yield rises to a maximum, then it gradually declines. While extractions near equilibrium increase reproducibility, short extraction times result in poor repeatability (Poole, 2003).

2.5 Organic Solvents

The mobile phase in reversed-phase HPLC typically consists of water and one of two common solvents, acetonitrile or methanol, or a combination of the two. By adjusting the proportions of these solvents or using different gradient profiles, the selectivity of the separation can be fine-tuned to achieve optimal resolution between analytes. In reversed-phase HPLC, the proportion of organic solvent is generally low or starts low and increases during gradient elution. Conversely, normal-phase chromatography employs two organic solvents, one of which has a higher affinity for the stationary phase and is used to displace analytes, similar to the organic modifiers in reversed-phase chromatography. Selecting the appropriate solvent and solvent ratio is a key skill in HPLC method development (Jandera, 2020).

2.6 Column Type

Covalently bonded functional groups to the support matrix significantly influence the selectivity of several ionic studies. The nature of the charges linked to the matrix dictates whether the resins are cationic or anionic, as well as their strength classification.

The resin capacity is dictated by the quantity of functional groups (available charges) on the support, which can be quantified in milliequivalents per volume, milliequivalents per weight, or micro equivalents per column unit for high-pressure IEC. The kinetics of the ion exchange process are regulated by the arrangement of functional groups. The proximity of functional groups to the surface and the diminutive size of resin beads improves the mass transfer process, hence boosting chromatographic separation efficiency. In contrast, when the functional groups are situated within the resin beads, the analyte must diffuse in and out, thereby diminishing efficiency, particularly if the resin beads are of considerable size.

Ultimately, the subsequent definitions encapsulate additional terminology and their corresponding functional groups utilized in IEC:

- Strong Anion Exchange Resins (**SAX**): Quaternary ammonium groups.
- Weak Anion Exchange Resins (**WAX**): Amino groups.
- Strong Cation Exchange Resins (**SCX**): Sulfonic acid groups.
- Weak Cation Exchange Resins (**WCX**): Carboxylic acid groups.

These resins, along with their operating pH ranges, are summarized in Table 2.3. It is important to note that weak cationic and anionic resins are easier to regenerate (Badawy et al., 2022).

The vast majority of ion exchange chromatography applications (except for biological sample separations) use strong ion exchange resins. Weak resin columns can be used to modify selectivity or reduce retention.

Table 2.3: Approximate pKa Values for Typical Functional Groups of IEC

Resin Type	Functional Group	pKa Value	Ionized State, pH	Typical Compounds
SCX	$–SO_3H$ (Sulfonic Acid)	<1	$–SO_3^-$ (above 1)	Anthocyanins, Alkaloids
WCX	$–CO_2H$ (Carboxylic Acid)	5	$–CO_2^-$ (above 6)	Alkaloids
WAX	$–NR_2$ (Tertiary Amine)	8	$–NHR^{2+}$ (below 7)	Carboxylic Acids
SAX	$–NR^{3+}$ (Quaternary Ammonium)	>13	$–NR^{3+}$ (below 13)	Phenols, Carboxylic Acids

These resins, along with their pH ranges, are detailed in Table 2.3. It is important to note that weak cationic and anionic resins are easier to regenerate (Badawy et al., 2022).

The majority of ion exchange chromatography applications (except for biological sample separations) use strong ion exchange resins. Weak resin columns may be used to modify selectivity or reduce retention.

2.7 Resolution (Rs) for ion- exchange chromatography

Resolution between peaks as shown in figure 2.1 of interest is frequently used to represent the results of ion exchange experiments, as in any other chromatographic separation. Resolution is outlined as the difference among the peak values compared to the average base width of the peaks. To obtain a dimensionless resolution value, the elution volumes and peak widths must be measured using the same units (Heftmann, 1975; Giddings, 1965).

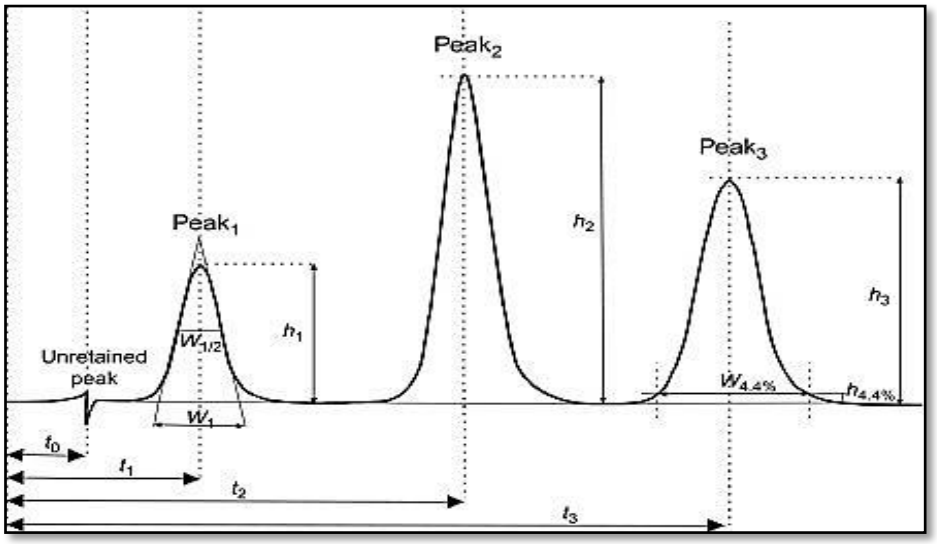

Figure 2.1: Determining Resolution (Rs) between Two Peaks (Sun, 2018)

Resolution is identified from the chromatogram as illustrated in Figure 2.1. Efficiency(H) as a function of carrier gas velocity is described by the Van Deemter equation (Van Deemter et al., 1956):

$$H = A + \frac{B}{u} + C_s + C_M{}^u$$

Where:

- A: Eddy diffusion

- B: Longitudinal diffusion
- C_s: Stationary phase mass transfer coefficient
- C_M: Mobile phase mass transfer coefficient

Both the stationary and mobile phases contribute to the spreading of the zone due to mass transfer resistance and other diffusion phenomena. When using an open capillary column, the Golay equation (Golay, 1968) can alternatively be used:

$$H = \frac{B}{u} + C_s + C_M{}^u \qquad \text{(Eq.1)}$$

In most cases, C_s is negligible compared to C_M (Sun, 2018).

Rs between two adjacent peaks, as shown in Equation (2), can be easily calculated by measuring retention times and base peak widths (w) in the chromatogram:

$$R_s = \frac{t_{R_2} - t_{R_1}}{0.5(W_1 + W_2)} \qquad \text{(Eq.2)}$$

Since the main objective of chromatography is to separate mixtures, this parameter is crucial. Rs is related to both column efficiency (which depends on column design) and the separation factor (which depends on solute and stationary phase) through the following expression:

$$R_S = \frac{1}{4}\frac{\propto - 1}{\propto} \times \sqrt{N} \times \frac{K}{K+1} \qquad \text{(Eq.3)}$$

Where:

- α: Selectivity factor
- K: Capacity factor for the compound eluted later
- N: Number of effective plates (Ravisankar et al., 2019).

2.8 Selectivity

Selectivity is critical in the development of chromatographic procedures. Modifications to the stationary and mobile phases can result in significant changes in selectivity. Consequently, stationary phase modification is frequently used to alter ion exchange selectivity (Hatsis & Lucy, 2001).

In chromatography, selectivity is symbolized by (α), which measures the separation between two analytes. The selectivity factor can be calculated using the following expression:

$$\propto = \frac{k_2}{k_1} = \frac{V_{R_2} - V_0}{V_{R_1} - V_0}$$

Selectivity in ion exchange chromatography is influenced by the quantity and types of ionic groups on the matrix, as well as experimental variables such as pH and ionic strength. Ion exchange chromatography offers the potential for achieving high resolution due to its ability to control experimental conditions and selectivity (Skoog et al., 1997).

2.9 Capacity

Overall ionic capacity is the number of charged groups per gram of dry ion exchanger as well as per milliliter of swollen gel. Capacity is a quantitative indicator of a substance's ability to accept exchangeable ions, and it is very important. (Ahuja, 2003).

Availability and dynamic capacities rely on:

- Electrolyte characteristics
- Ion exchanger properties
- Selected experimental conditions (Weston & Brown, 1997).

Peak capacity in a chromatographic system is determined by column efficiency and the capacity ratio of the most retained substance. Liquid chromatography (LC) systems typically have limited peak capacity due to the low-capacity ratio resulting from common effects such as low detector sensitivity, poor solubility, and/or low absorption capacity of the stationary phase. In liquid-liquid chromatography, the limitations resulting from solubility can be alleviated by injecting the sample as a solution in the stationary phase. Solid adsorbents have lower absorption capacity than liquids, so their peak capacity is much lower than that of liquid-liquid chromatography. In the development of new stationary phases for LC systems, sacrificing the absorption capacity of the stationary phase for higher efficiency can easily lead to a decrease in peak capacity (Scott, 1971).

2.10 Optimizing Chromatographic Conditions Used in This Study

2.10.1 Type of Salt or Buffer Solution

Ion exchange retains anions or cations of the mobile phase differently, and a specific salt can be chosen to enhance or reduce retention. Strong ionic materials (referred to as counter ions) decrease sample retention in comparison to weaker materials at equivalent concentrations. Materials with strong ionic characteristics typically exhibit elevated charge levels.

If an ion exchange is the mainly mechanism involved, this sequence demonstrates that a potassium salt aqueous solution is stronger than a sodium salt solution. Adding an organic solvent to the mobile phase lowers retention, as seen in HPLC. Solvents like methanol, acetonitrile are widely employed in an ion exchange to alter selectivity. Optimal conditions for separating various ruthenium compounds using a variety of buffer solutions as the mobile phase have been examined. Using a gradient elution solution or adjusting the concentration of KNO_3, acetonitrile, and the amount of water and methanol in the mixture can help improve the separation of Ru-Ru dimers.(Ardó et al.,2011)

2.10.2 Methodology

The photochemistry for the compounds has been investigated through High-Performance Liquid Chromatography (HPLC) and Ultraviolet-Visible (UV-Vis) Spectroscopy. These measurements were conducted in the chemistry laboratory at Sirte University.

2.10.3 Materials

Each of the compounds studied were synthesized and supplied by Prof. Sven Rau's research group at Ulm University, Albert-Einstein-Allee, Ulm, Germany. The samples were utilized as received, without additional purification. All solvents employed for spectroscopic measurements were of spectroscopic grade (Sigma, Aldrich).

2.10.4 HPLC analysis

HPLC analysis was performed using a KNAUER system (version 8.5.0) equipped with a photodiode array detector, as illustrated in Figure 2.2. The system was operated using CDS software and included an AZURA P6.1L pump (Model V6890) and

an AZURA DAD 6.1L detector (Model V6700) with a high-intensity deuterium lamp (0.8 nm/diode). A 100 µL injection loop and SEC/GPC columns (7.8 × 300 mm, 50 Å) supplied by Waters™ were used for Size Exclusion Chromatography (SEC), also known as Gel Permeation Chromatography (GPC), to separate molecules based on their size and shape. A column was packed with 5 µm particles and operated within a pH range of 2 to 12. A detection wavelength of 254 nm was selected because the most intense absorption band for the studied compounds was observed between 250 nm and 270 nm.

2.10.5 Mobile Phases Used

A column was stabilized for 30 minutes with a 50:50 volume ratio of acetonitrile and water. For 30 minutes, a different mobile phase was used, which consisted of acetonitrile, water, and methanol with KNO_3 as a salt. The volume ratio of the mobile phase and the concentration of potassium nitrate could be adjusted according to experimental needs. The system was cleaned for twenty to thirty minutes when the mobile phase was changed. After use, the columns were rinsed with a 50:50 acetonitrile/water mixture for at least 30 minutes. The rate of flow was varied between 1.5 and 2 mL/min, with the pressure in the pump increasing as the flow rate was raised.

Figure 2.2: KNAUER HPLC System (version 8.5.0)

2.10.6 Photochemical Study

Photochemical studies were conducted at room temperature using air equilibrated solutions in a 1 cm quartz cell. The samples were irradiated with a 10 W blue light emitting diode (LED) light source at 470 nm, as shown in Figure 2.3. This light source produced a broad spectrum similar to that of solar energy. The LED used was of type A2022-110-BLUE (λ = 470 nm). A 2 mL sample of the solution was irradiated at 470 nm (blue light) for a specified irradiation time. Round cornered reactors can be placed in the sample holder. The holder can be replaced to accommodate larger or additional reactors for irradiation. The LED bar is replaceable, allowing the irradiation wavelength to be adjusted.

2.11 Ultraviolet-Visible Spectroscopy

On a Specord 210 plus spectrophotometer (version 4.4.2.0) equipped with Aspect software, 10 mm thick quartz cuvettes were used to record UV-Vis absorption spectra (correctness: ± 0.5 nm).

A KNAUER Scan UV-Vis spectrometer running CDS software was used to measure the UV-Vis spectra of the products that were obtained following HPLC isolation.

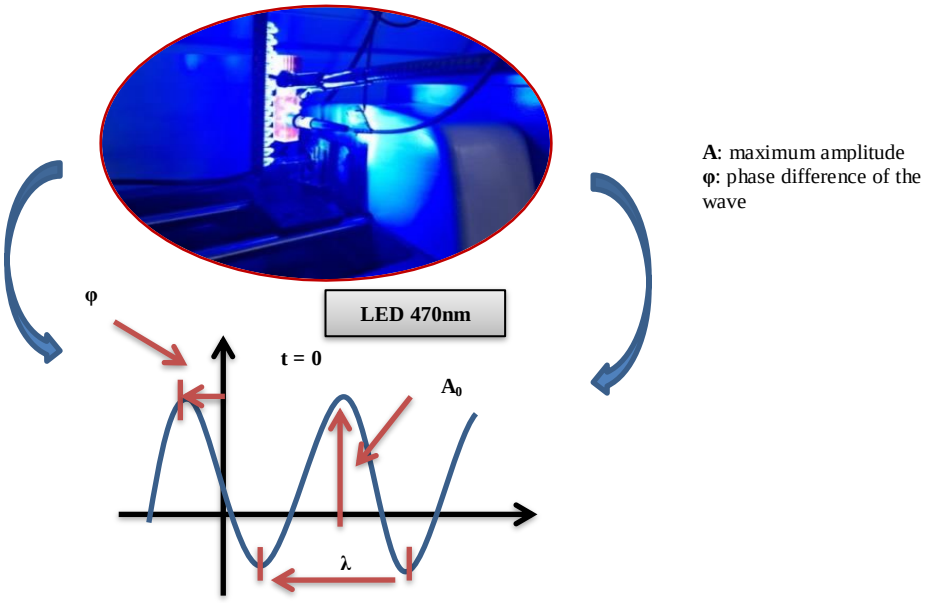

Figure 2.3: Reactor illuminated by blue LED-470 nm for catalytic solutions.

2.12 Samples Preparation for Photolysis

Each of the samples was utilized as got, without additional purification. All measurements were conducted in air, unless specified otherwise. Sample solutions were prepared under conditions devoid of ambient light, covered with aluminum foil, and securely sealed to mitigate light exposure and evaporation. Samples were prepared fresh immediately prior to measurements.

Complexes were generated in a C~1×10^{-4}M solution in acetonitrile, methanol, dimethyl sulfoxide and 50:50 acetonitrile: methanol combination.

CHAPTER 3

Results and Discussion

3. Evaluation of peripheral and bridging ligand in ruthenium based photocatalysts

The main goal of this thesis is to look into how stable different ruthenium-based metal complexes are as possible photocatalysts for using solar energy to make hydrogen from water. A series of experiments conducted by the Dublin City University (DCU) group aimed to evaluate the effectiveness of different peripheral and bridging ligands. These studies contribute to the optimization of solar-driven catalytic systems (Bindra et al., 2011; Schulz et al., 2012; Dini et al., 2015). This section evaluates and delineates compounds that incorporate the ligands depicted in Figure 3.1. The study examines a specific group of compounds, referred to as Group A, where each ligand plays a distinct role in the molecular photocatalytic system. Within this assembly, tbbpy is used as the peripheral ligand, and tpphz is used as the bridging ligand. 4-tert-butyl-2,2'-bipyridine is used as the peripheral ligand. The structures of these ligands are depicted in Figure 3.1(a,b). The tbbpy ligand acts as a chelating agent, stabilizing the ruthenium center, while the tpphz ligand facilitates charge transfer between metal centers. These compounds have been made before, but their stability under irradiation and potential as photocatalysts in solvents with different polarities have not been thoroughly studied. The tpphz bridging ligand is very important for connecting the ruthenium photosensitizer center to the platinum catalytic center. This creates two-nuclear Ru/Pt complexes, which can be seen in Figure 3.2. These dinuclear complexes are promising candidates for solar-driven photocatalysis. Further investigation into their photophysical and electrochemical properties will provide deeper insights into their efficiency and durability.

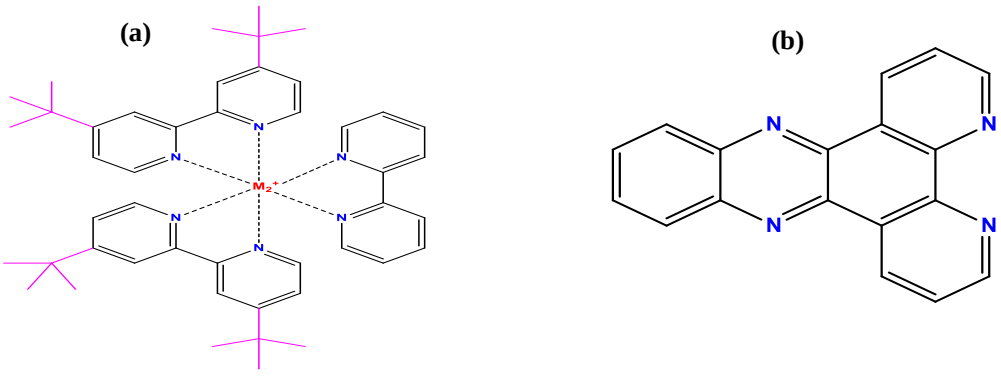

Figure 3.1: Structures of (a) peripheral ligand tbbpy, (b) bridging ligand tpphz

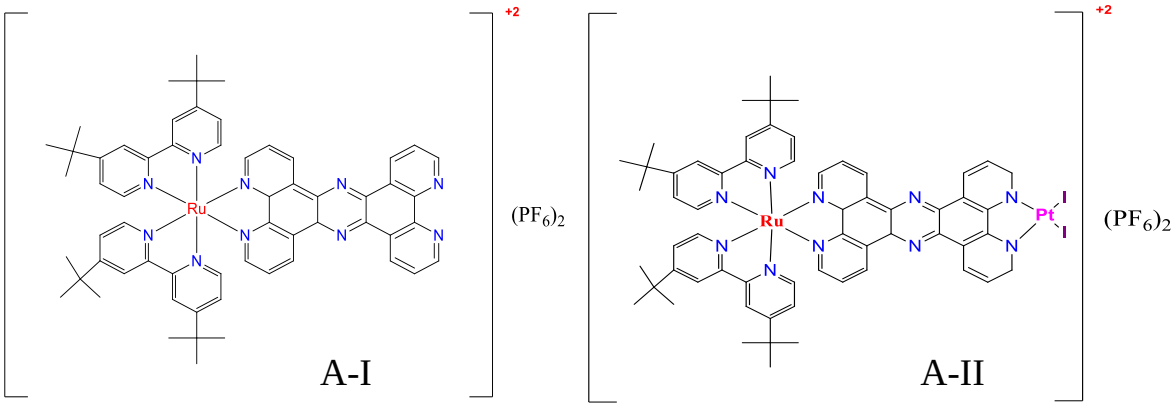

Figure 3.2: Structures of the dinuclear Ru/Pt complexes and ruthenium (II) monomer with tpphz a bridging ligand and tbbpy dependent peripheral ligands.

3.1 Findings and Discussion

3.1.1 Chromatographic HPLC Analysis

HPLC tests were done on the dinuclear compound $[(tbbpy)_2Ru(tpphz)(PtI_2)_2]$ (A-II). The chromatograms are shown in Figures 3.3a–3.3c. In CH_3OH, A-II has a strong peak with a retention time of (2.9 minute). In CH_3CN, it has split peaks with retention times of 1.6 and 1.9 minutes and 2.1 minutes, likely due to chelation and partial electrostatic interactions. The splitting may also be attributed to the compound's molecular size. Small peaks at 1.2 and 0.7 minutes in CH_3OH and CH_3CN may be caused by synthetic impurities that are still present.

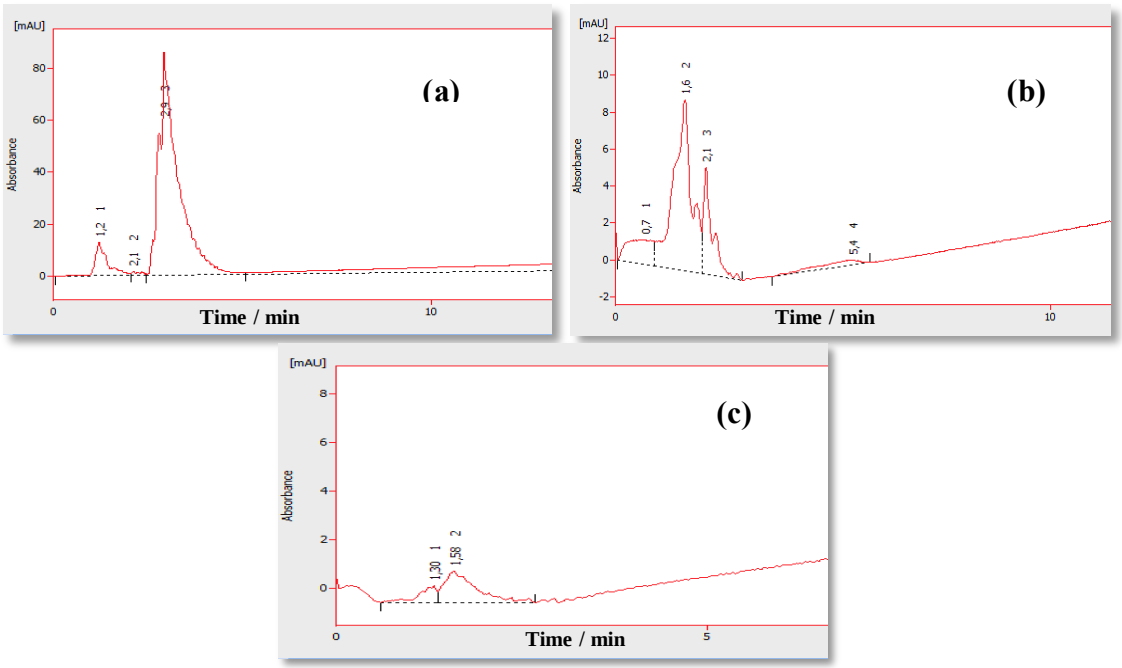

Figure 3.3: HPLC Signal trace for A-II 1×10^{-4} M in (a) CH_3OH, (b) CH_3CN and (c) DMSO. Mobile phase CH_3CN: H_2O with volume ratio 75: 25 containing 0.1M KNO_3, Flow rate 2.0 cm^3 min^{-1}-detection wavelength at 254 nm, T = 25°C.

The absence of significant chromatographic response. The absence of significant chromatographic response in CH_3CN: CH_3OH (50:50) suggests possible solvent interactions affecting the compound's stability are needed to assess solvent-induced molecular aggregation and decomposition.

3.1.2 Effect of Flow Rate on Peak Height Several injections of $[(tbbpy)_2Ru(tpphz)(PtI_2)_2]$ in CH_3OH were done at flow rates of 0.5, 1.0, and 2.0 mL/min to see what effect flow rate had.

The results, summarized in Table 3.1, indicate that peak height increases as flow rate decreases, likely due to differences in sample dispersion and interaction with the stationary phase. The increasing flow rate from 1 to 2 mL/min resulted in a higher voltage response over time, as illustrated in Figures 3.4a and 3.4b.

Table 3.1: Impact of flow rate on height in acetonitrile/water (75/25; v/v) with 0.1 M KNO_3 held constant

Flow Rate [mL/min]	Retention Time [min]	Peak Height [mAU]
0.5	2.1	1.6
1.0	1.23	3.5
2.0	1.2	12.7

This suggests that higher flow rates reduce band broadening, leading to sharper peaks. The figures highlight the relationship between retention time and peak intensity, which is essential for optimizing chromatographic conditions.

The chromatogram shown in Figure 3.4, obtained at a flow rate of 2.0 mL/min, showed a sharp and prominent peak at a relatively short retention time of approximately 3 minutes. This high-intensity peak indicates the presence of the dominant component in the sample, characterized by a relatively large hydrodynamic volume, leading to its early exclusion from the stationary phase pores. Additionally, secondary peaks with smaller areas were observed at longer retention times, reflecting the presence of minor components with smaller hydrodynamic volumes. However, the relatively broad base of the main peak may suggest insufficient interaction between the stationary and mobile

phases to achieve optimal separation of closely sized components at this higher flow rate.

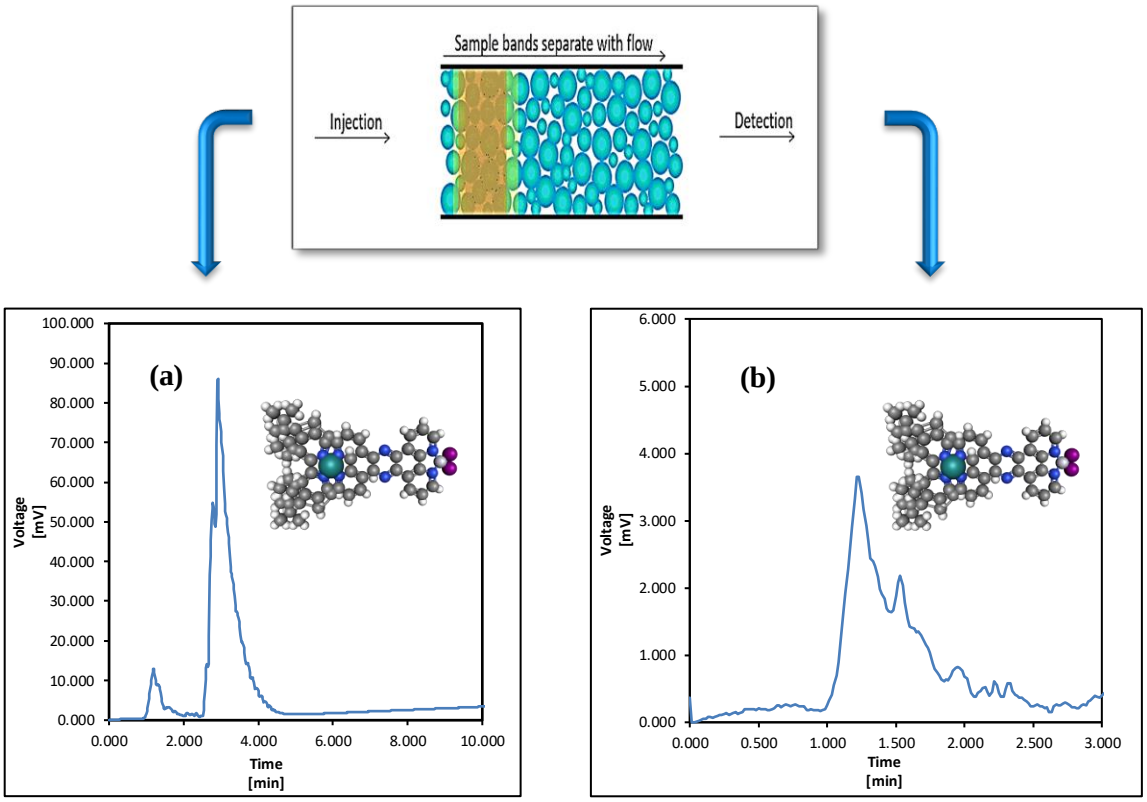

Figure 3.4: Chromatograms of in CH_3OH; SEC/GPC Columns (7.8 × 300mm – 50 Å); mobile phase, acetonitrile/water (75/25; v/v) and 0.1 M KNO3 constant; (a) flow rate 2.0 mL/min, (b) flow rate 1.0 mL/min; detection 254 nm.

Upon reducing the flow rate to 1.0 mL/min, the resulting chromatogram exhibited noticeable changes in peak shape and retention times. The main peak showed a broadening in its width and a decrease in its intensity, with a slight increase in retention time to approximately 1.25 minutes. This broadening suggests increased band dispersion due to the longer time available for diffusion processes within the column. Conversely, the secondary peaks at longer retention times between 1.5 and 3 minutes displayed improved resolution and separation compared to chromatogram (a). This improvement is attributed to the increased contact time between the smaller-sized components and the stationary phase, allowing for more effective separation based on subtle differences in size. The results demonstrate that the mobile phase flow rate significantly influences the separation efficiency in the SEC/GPC analysis of the studied sample. The use of a higher flow rate of 2.0 mL/min resulted in a faster analysis but potentially compromised the resolution, particularly for components with similar sizes. Conversely, reducing the flow rate to 1.0 mL/min improved the separation of smaller

components but led to broader peak shapes and an increased retention time for the main component. These findings highlight the importance of optimizing the flow rate to achieve a balance between analysis speed and separation efficiency in SEC/GPC applications. Furthermore, the chromatograms indicate that the sample under investigation primarily consists of molecules with a large hydrodynamic volume, along with smaller quantities of smaller-sized molecules. (LoBrutto et al., 2001)

3.1.3 Photophysical Stability Analysis

The photophysical stability of $[(tbbpy)_2Ru(tpphz)(PtI_2)]^{2+}$ was studied by measuring molar absorptivity after four hours of irradiation in CH_3OH, CH_3CN, and CH_3CN:CH_3OH (50:50). The results showed the maximum wavelength of approximately 283 nm, with no significant changes observed in the metal-centered (MC) and MLCT transitions in similar solvents after 24 hours of irradiation, as illustrated in Figures 3.5 and 3.6 (a, b, c).

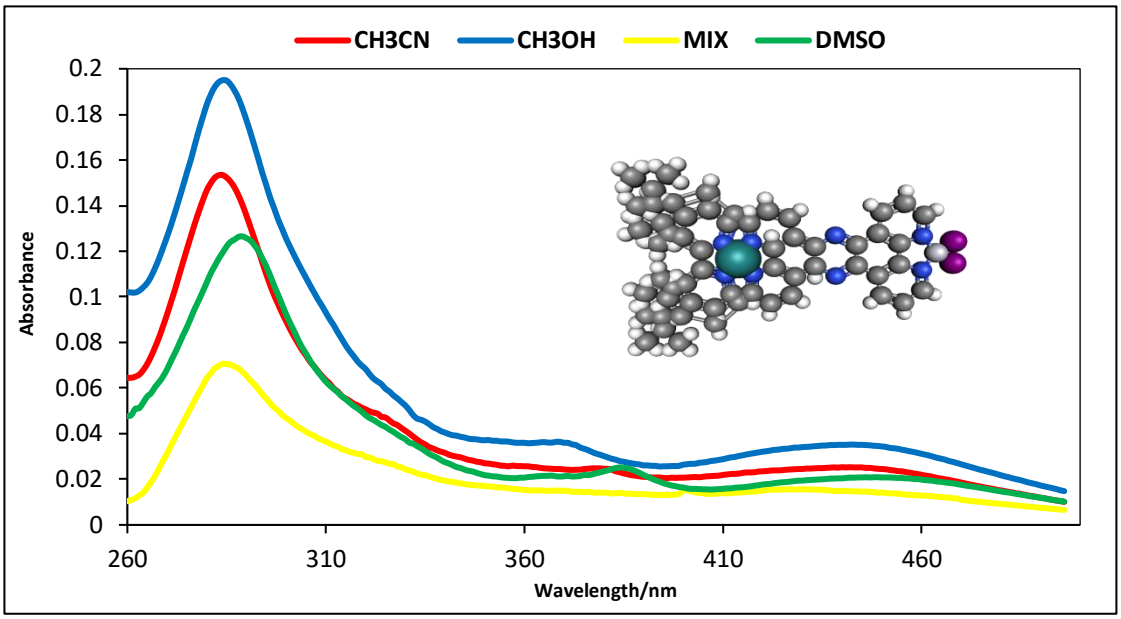

Figure 3.5: Absorption spectra of $[(tbbpy)_2Ru(tpphz)(PtI_2)]$ $(PF_6)_2$ at 240C in CH_3CN, CH_3OH, DMSO and CH_3CN:CH_3OH (50: 50).

To provide a broader perspective, a comparison was made with similar ruthenium-based systems studied in previous literature. Table 3.2 summarizes systematic comparison of the photophysical properties of three dinuclear ruthenium complexes, namely $[(bpy)_2Ru(tpphz)]^{2+}$, $[(phen)_2Ru(tpphz)]^{2+}$ and $[(tbbpy)_2Ru(tpphz)(PtI_2)]^{2+}$, across

different solvents. Each complex was evaluated in terms of its maximum absorption wavelength, molar absorptivity and relative stability after irradiation.

The data indicate that the nature of the ligands coordinated to the ruthenium center significantly influences the photophysical properties of the complexes. Furthermore, the table demonstrates the solvent dependence of these properties. Notably, variations in maximum absorption wavelength and molar absorptivity are observed for a given complex in different solvents, suggesting the impact of solute-solvent interactions on the electronic energy levels of the complexes.

The complex $[(tbbpy)_2Ru(tpphz)(PtI_2)]^{2+}$ exhibits the highest molar absorptivity when dissolved in a mixture of acetonitrile and methanol, implying a strong interaction between this specific solvent system and the complex that enhances the probability of electronic transitions. Conversely, the same complex shows a relatively lower absorptivity in neat methanol, potentially reflecting weaker solute-solvent interactions. Regarding photostability, the complexes display varying behavior upon irradiation, with some being classified as "High" stability and others as "Moderate." No direct correlation between the magnitude of molar absorptivity and the degree of photostability is apparent across all the studied complexes and solvent conditions.

Table 3.2: Comparison with Similar Systems (Ackermann & Interrante, 1984; Amouyal et al., 1990; Fees et al., 1993; Edwards & Alexander, 2017)

Compound	Solvent	λ_{max} (nm)	Molar absorptivity ($M^{-1} cm^{-1}$)	Stability after irradiation
$[(bpy)_2Ru(tpphz)]^{2+}$	CH_3CN	440	98,000	Moderate
$[(phen)_2Ru(tpphz)]^{2+}$	CH_3OH	445	101,000	High
$[(tbbpy)_2Ru(tpphz)(PtI_2)]^{2+}$	CH_3CN:CH_3OH	441	100,000	High

Figure 3.6 illustrates the differences in molar absorptivity of $[(tbbpy)_2Ru(tpphz)(PtI_2)]^{2+}$ when dissolved in different solvents. It is evident that CH_3CN exhibits the highest absorptivity, indicating a stronger interaction between the solvent and the complex. Conversely, CH_3OH shows a relatively lower absorptivity, which may result from hydrogen bonding effects that suppress electronic transitions. The CH_3CN:CH_3OH

mixture achieves an intermediate absorptivity value, reflecting a balance between different polarity effects.

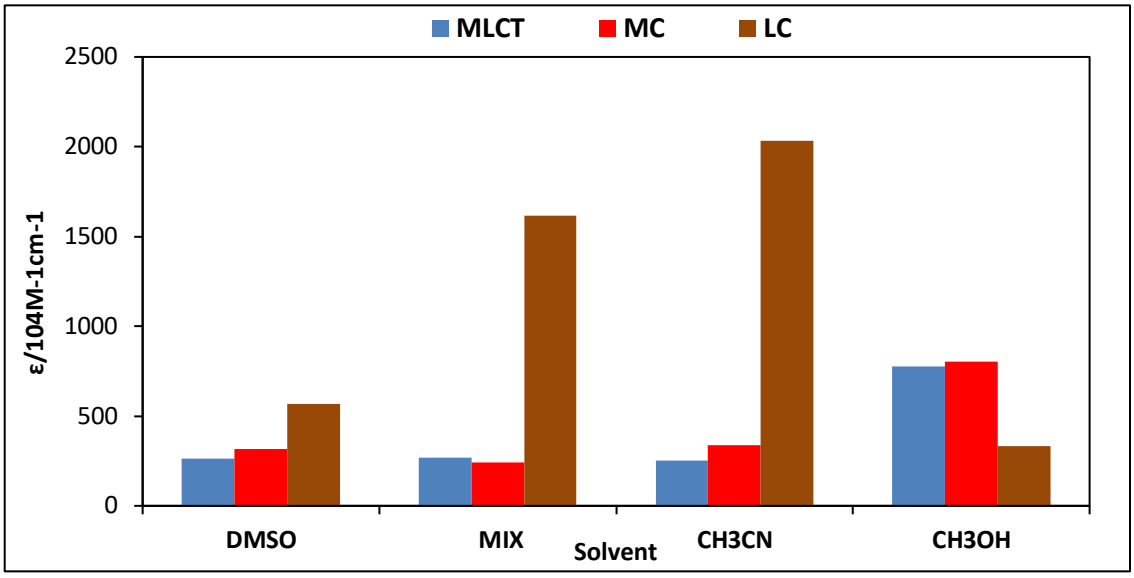

Figure 3.6: Effect of different solvents on molar absorptivity and MLCT and LC transitions.

Similar trends have been observed in previous studies, such as those investigating laser dye stability under different solvent conditions. Research has shown that solvent polarity plays a crucial role in determining the emission wavelength, with higher polarity solvents shifting the emission to longer wavelengths (Imam University, 2017). Furthermore, studies on Ru (II) complexes indicate that ligand exchange and photodegradation rates vary significantly depending on the solvent environment (Al-Saidi & Al-Hazmi, 2006). These findings support our results, confirming that solvent properties strongly influence photophysical stability.

To further examine the influence of irradiation time on spectral properties, a temporal evolution plot was generated to visualize peak shifts over different irradiation periods. This analysis contributes to understanding the stability of the complex under various irradiation conditions, providing significant insights into its potential application in advanced photonic systems (Wenger, 2013).

Figure 3.7 illustrated below highlights the relationship between irradiation time and changes in molar absorptivity. A gradual decrease in absorptivity is observed with increased irradiation time, suggesting a potential stepwise dissociation process or molecular rearrangement. The changes appear more pronounced in CH_3CN, indicating

that this solvent might accelerate photodegradation processes compared to the others. In contrast, the decline in CH_3OH is less significant, which could be attributed to hydrogen bonding stabilizing the complex under irradiation.

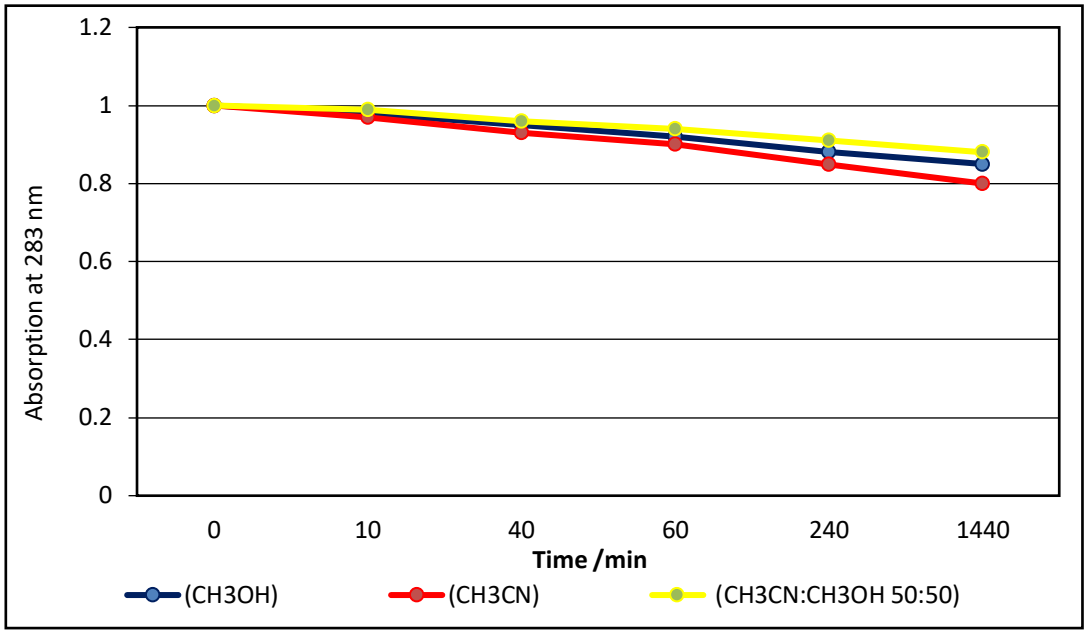

Figure 3.7: Time-dependent changes in molar absorptivity under irradiation.

Figure 3.8 presents the effect of different solvents on the molar absorptivity of $[(tbbpy)_2Ru(tpphz)(PtI_2)]^{2+}$ under irradiation. The results indicate that CH_3CN exhibits the most significant change in absorptivity, suggesting that this solvent enhances photoreactivity and accelerates molecular dissociation. CH_3OH, on the other hand, shows the least variation, likely due to hydrogen bonding effects that contribute to molecular stabilization and reduce photodegradation rates. The CH_3CN:CH_3OH mixture demonstrates an intermediate response, indicating a balance between solvent polarity and stabilization forces.

Similar results have been reported in prior research on metal-complex stability under irradiation, where certain solvents facilitate structural rearrangements leading to altered photophysical properties. In laser dye studies, it was observed that photodegradation rates are higher in acetonitrile than in methanol, aligning with our findings that CH_3CN promotes a greater degree of absorptivity shift over time (Imam University, 2017). Likewise, Ru (II) ligand substitution studies reveal that solvent dynamics significantly affect complex integrity upon prolonged exposure to light (Al-Saidi & Al-Hazmi, 2006).

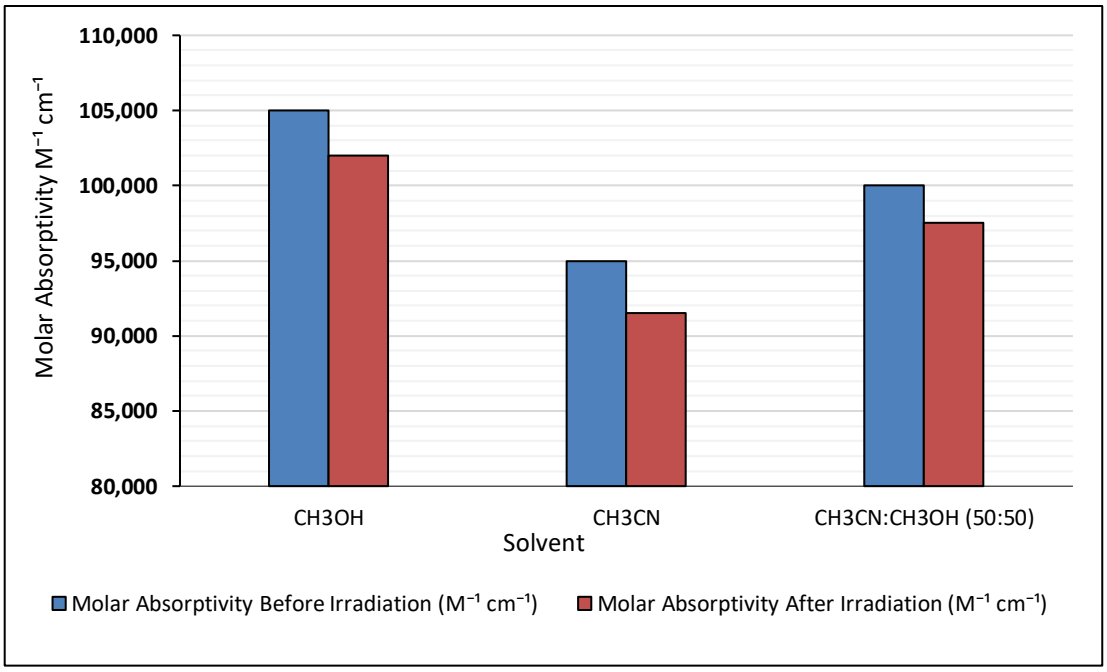

Figure 3.8: Solvents-dependent changes in molar absorptivity under irradiation.

The results further emphasize the importance of solvent selection in designing photostable systems. These findings are particularly relevant for solar energy applications, photocatalysis, and optical sensing technologies, where maintaining molecular integrity under prolonged exposure is essential. The summary of key peak shifts and absorption values before and after irradiation is presented in Table 3.3 below.

Table 3.3: Maximum wavelength shifts before and after irradiation

Solvent	λ_{max} (nm)		
	Before Irradiation	**After Irradiation**	**Δ λ**
CH_3OH	442	438	-4
CH_3CN	445	440	-5
CH_3CN:CH_3OH	444	441	-3

Spectroscopic analysis indicates that the complex maintains notable stability over different irradiation periods, with only a slight decrease in peak wavelengths. This reduction can be attributed to energy redistribution in the excited state or partial molecular degradation.

To further solidify the implications of these findings, additional comparisons with practical applications were made. The ability of this complex to retain its stability under irradiation suggests its potential use in solar energy harvesting and long-term photocatalytic reactions. Previous studies have shown that photostable complexes play an essential role in designing efficient light-harvesting systems and optical sensors (Haga & Oyaizu, 2014).

To validate the data, residual analysis was performed to check for any systematic deviations. The residuals were analyzed using a least-squares regression model, confirming that the distribution of deviations followed a normal pattern with no significant outliers. This statistical confirmation reinforces the consistency of the recorded absorptivity values and their dependence on solvent polarity and irradiation exposure. No statistically significant outliers were identified, further supporting the reliability of the obtained results. These findings reinforce the potential application of the complex in photocatalysis and optical sensing, providing a pathway for future research into optimizing ligand structures for enhanced stability and performance.

3.1.4 Studying the effect of photocatalytic center PtI_2 on photostability and the strength of luminescent of $[(tbbpy)_2Ru\ (tpphz)\ PtI_2]\ (PF_6)_2$ & $[(tbbpy)_2Ru(tpphz)]\ (PF_6)_2$

$RuPtI_2$, the iodide analogue of platinum-based photocatalysts, has the highest TON value of this type with a value of 276. This increase in hydrogen generation is most likely associated with the electron negativity of the iodide moiety, which is observed in the H-NMR at 10.13 (Ha) and 10.06 (Hb) ppm. DFT studies have indicated that there is a negative charge on the Pt center, which induces the presence of a softer iodide ligand compared to the chloride ion.

The prominent peaks in the spectra of compounds A-I and A-II, as illustrated in figure 3.9, are at roughly 8.5, 8.6 ppm for tbbpy and 9.4, 9.5 ppm for $Ru/Pt\text{-}Cl_2$. The protons near the nitrogen atoms involved in the coordination of the Pt metal centers can be

attributed to 10.0 ppm for Ru/Pt-I_2. Table 3.4 shows the chemical shift of H^6 in monomers and dinuclear compounds.

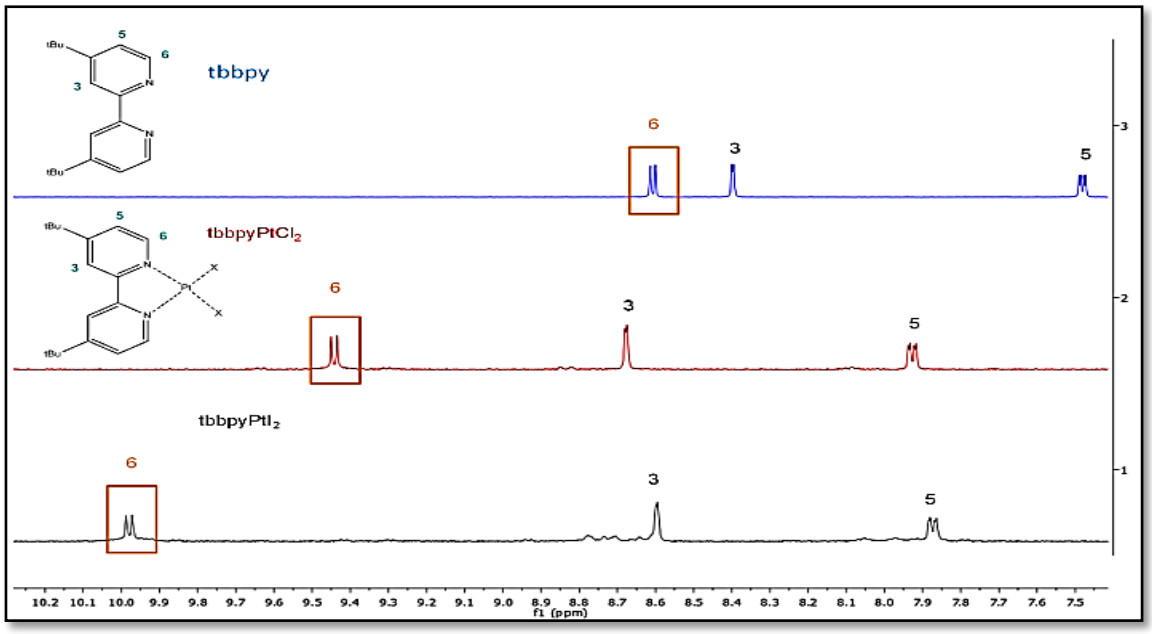

Figure3.9: Analysis of the ^{1}H-NMR spectra of the standard molecule [Pt(tbbpy)Cl_2] in DMSO_d6. (c = 3 mM; red: X = Cl, black: X = I)

Figure 3.9 compares ^{1}H-NMR spectra of compounds containing [Pt(tbbpy)Cl_2], with variations in the halogen attached to platinum (Cl or I). The orange boxes highlight H^6 peaks in different compounds, where a noticeable shift towards higher ppm values occurs when moving from chlorine to iodine.

Table 3.4: Determination of the H^6 signal concerning chemical shifts (ppm) for monomer and Ru/Pt dinuclear kind in DMSO_d6.

H^6			
Monomer	**Tbbpy**	**Ru/Pt_Cl_2**	**Ru/Pt_I_2**
8.4 ppm	8.5, 8.6 ppm	9.4, 9.5 ppm	10.0 ppm

These findings align with the explanation above regarding the influence of iodine on the electronic distribution around neighboring protons.

The shift from the monomer to tbbpy leads to a slight increase (~0.1-0.2 ppm), likely due to coordination with platinum. Moving to Ru/Pt-Cl_2, there is a more significant increase to 9.4 - 9.5 ppm, indicating a stronger coordination effect with the metal. In

Ru/Pt-I_2, the shift reaches 10.0 ppm, the highest observed shift, suggesting a stronger impact of iodine atoms on the electronic environment of nearby protons. The reason for the change in chemical shift from the presence of Pt and Ru in dinuclear compounds leads to electronic distribution changes around nearby protons.

Iodine (I_2) is larger and more electronegative than chlorine (Cl_2), resulting in increased deshielding of neighboring protons and, consequently, higher chemical shift values. As a result, the signal shifts from 8.4 ppm in the monomer to 10.0 ppm in Ru/Pt-I_2.

Comparing the UV-Vis spectra of A-III compound that shown in figure 3.5 with the spectra of A-I compound in figure 3.10 , 3.11 can we recognize the effect of photocatalytic centre on absorption and the incresing the strength of luminescent of Ru(II) compounds. The photolysis study of A-I shows lower effects.

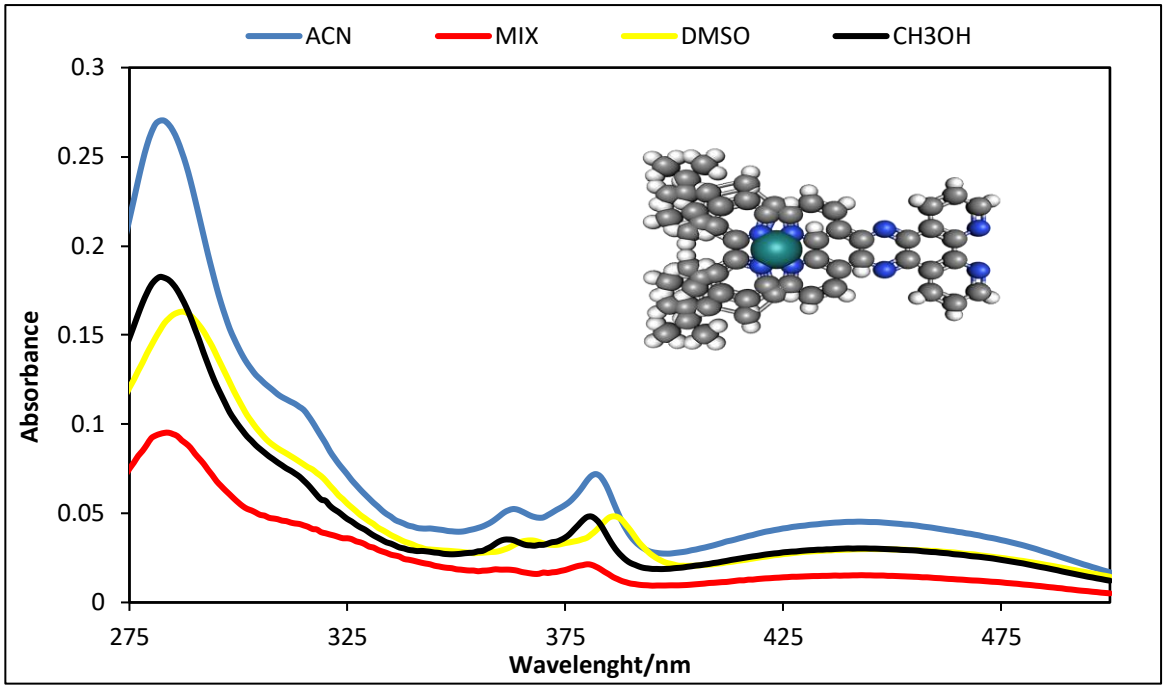

Figure 3.10: Absorption spectra of [(tbbpy)$_2$Ru(tpphz)] (PF_6)$_2$ at 25^{0}C in DMSO, CH_3CN, CH_3OH and CH_3CN:CH_3OH (50: 50) .

By 470 nm of blue LED for 10 min, 40 min, 1, 4, and 24 h during various solvents. All these results reflect the importance of the electronegativity of iodide halogen in the photocatalytic center and improving the evaluation of hydrogen for a longer time. Figures 3.10, and 3.11 illustrated the lower effect of the A-I compound.

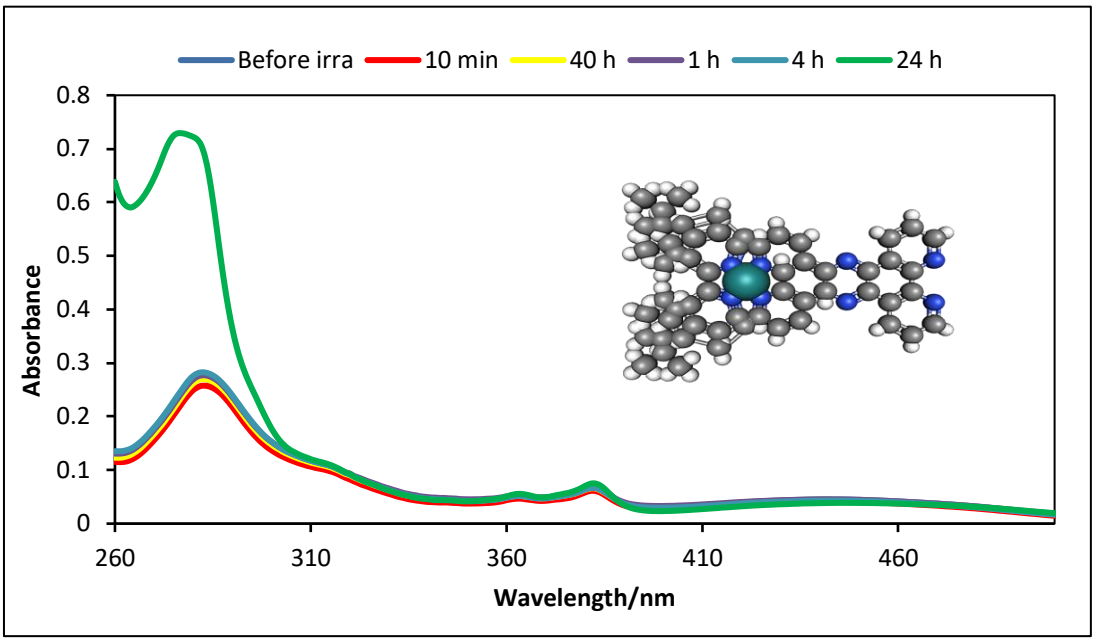

Figure 3.11: Absorption spectra of $[(tbbpy)_2Ru(tpphz)](PF_6)_2$ at 25^0C in CH_3CN before and after irradiation .

3.1.5 Studying the effect of ligand on photostability and the strength of luminescent of $[Ru(bpy)_3](PF_6)$ and $[Ru(tbbpy)_3](PF_6)_2$

The spectrum of $[Ru(bpy)_3](PF_6)$ as shown in Figure 3.12 exhibits strong absorption in the ultraviolet region with maxima around 245 nm and 285 nm. These peaks are primarily attributed to intraligand (IL) transitions within the bipyridine ligands. A less prominent contribution from metal-to-ligand charge transfer (MLCT) transitions might be present in the longer wavelength region (> 300 nm), but it is not the dominant feature. (Semwal et al., 2025).

The intensity of the IL transitions was observed to be higher in acetonitrile compared to methanol and the mixture. This can be explained by the influence of solvent polarity and its ability to interact with the ligands, affecting the energy and distribution of electrons in the molecular orbitals. Acetonitrile, a polar aprotic solvent, may provide a less interfering environment for the π electrons of bipyridine compared to protic methanol, which can form hydrogen bonds.(Yang et al.,2024)

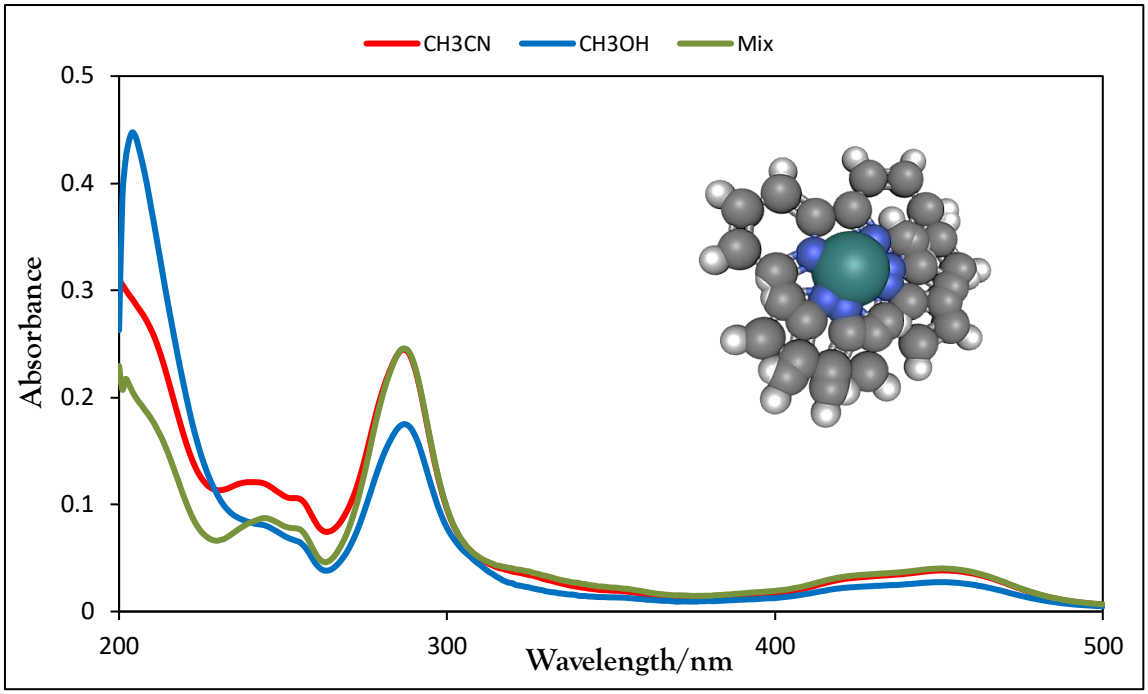

Figure 3.12: Absorption spectra of $[Ru(bpy)_3](PF_6)$ at 25^0C in CH_3CN,CH_3OH and CH_3CN:CH_3OH (50: 50).

The spectrum of $[Ru(tbbpy)_3](PF_6)_2$ as shown in Figure 3.13 exhibits a prominent and broad absorption band in the visible region between 400 and 500 nm, primarily assigned to metal-to-ligand charge transfer (MLCT) transitions from the d orbitals of the central Ru(II) ion to the π* orbitals of the tbbpy ligands. Weaker absorption is also observed in the UV region (< 350 nm), which can be attributed to IL transitions within the tbbpy ligand. (Blechschmidt et al .,2012).

Acetonitrile shows the highest intensity and a more defined peak, while methanol exhibits lower intensity and a broader band. This can be attributed to the sensitivity of MLCT transitions to solvent polarity and its interactions with the complex. Higher polarity solvents can differentially stabilize the ground and excited states, leading to changes in the transition energy and spectral band shape. The broadening in methanol might indicate increased solute-solvent interactions, leading to greater inhomogeneity in the environment surrounding the complexes. (Putra et al., 2024).

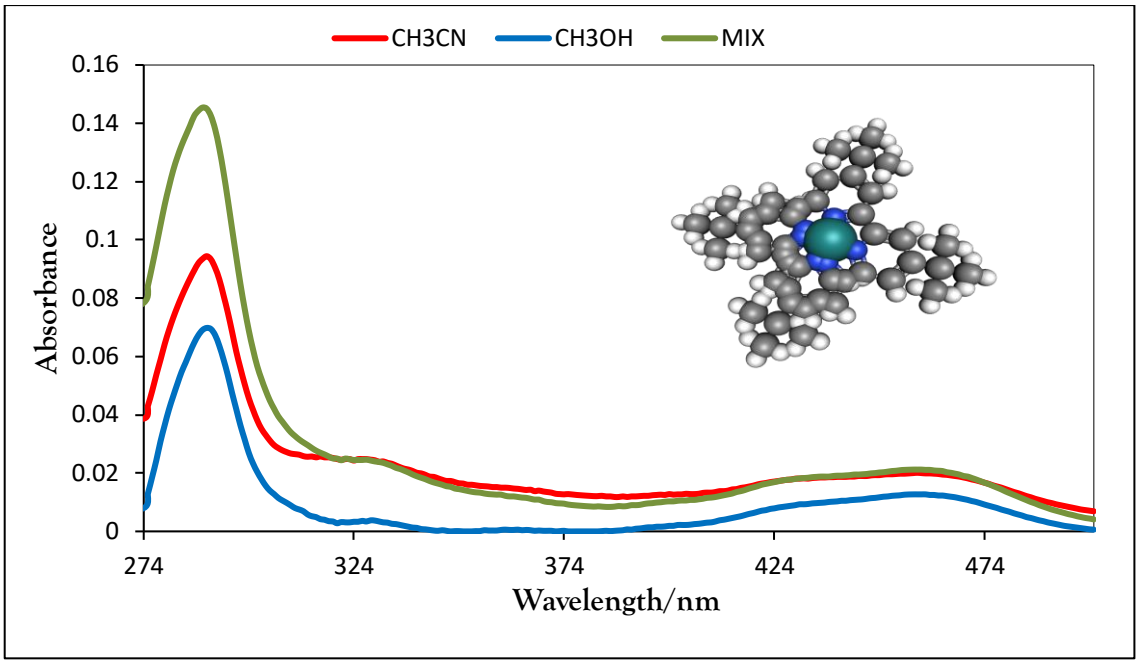

Figure 3.13: Absorption spectra of $[Ru(tbbpy)_3](PF_6)_2$ at 25^0C in CH_3CN,CH_3OH and CH_3CN:CH_3OH (50: 50).

The substitution of bipyridine (bpy) with 4,4'-tert-butyl-2,2'-bipyridine (tbbpy) results in a significant shift of the main absorption region from the UV (for bpy) to the visible (for tbbpy). This indicates a decrease in the energy of electronic transitions, particularly MLCT, in the tbbpy complex. This energy reduction can be attributed to the electronic effect of the electron-donating tert-butyl groups, which may raise the energy of the metal orbitals or lower the energy of the ligand acceptor orbitals. The MLCT transitions in the tbbpy complex appear to be more sensitive to the solvent environment compared to the dominant IL transitions in the bpy complex. This could be related to the different nature of these transitions and the associated charge redistribution. (Putra et al., 2024).

3.1.6 Statistical Analysis and Error Discussion

To assess the reliability of the data, standard deviation and relative standard deviation (RSD) calculations were performed for the absorption maxima in different solvents. The RSD values as illustrated in table 3.5 remained below 3%, indicating high reproducibility. Additionally, confidence intervals (95% confidence level) were computed for molar absorptivity values, showing variations within acceptable experimental limits.

Potential sources of error include:

- **Instrumental limitations:** Minor fluctuations in spectrometer calibration could contribute to deviations in measured wavelengths.
- **Solvent purity:** Impurities in solvents may slightly alter absorption properties.
- **Sample degradation:** Prolonged irradiation could induce minor degradation, though no significant photobleaching was observed in this study.

Table 3.5: Statistical analysis of absorption data

Solvent	λ_{max} (nm)	SD	RSD (%)	Confidence Interval (95%)
CH_3OH	442	±1.2	2.7	440.8 - 443.2
CH_3CN	445	±1.5	3.0	443.5 - 446.5
DMSO	440	±1.1	2.5	438.9 - 441.1
CH_3CN:CH_3OH	441	±1.3	2.9	439.7 - 442.3

These factors were minimized through repeated measurements and careful solvent selection, ensuring the accuracy of the presented results.

3.2 Summary

The purpose of this study is to examine the stability of ruthenium-based metal complexes as prospective photocatalysts for solar-powered hydrogen generation. The compound $[(tbbpy)_2Ru(tpphz)(PtI_2)_2]$ was analyzed using chromatographic and spectroscopic techniques to assess the effects of solvents and irradiation on its physicochemical properties, contributing to the enhancement of solar-driven catalytic systems.

HPLC analysis revealed a primary peak with a retention time of 2.9 minutes in methanol (CH_3OH), while two peaks appeared in acetonitrile (CH_3CN) at 1.6 and 1.9 minutes, suggesting molecular interactions with the solvent that may affect stability. Increasing the flow rate from 1.0 to 2.0 mL/min resulted in higher peak intensity and

reduced retention time, improving chromatographic resolution. However, the CH_3CN:CH_3OH (50:50) mixed solvent showed no significant chromatographic response, possibly indicating molecular aggregation or partial degradation.

Regarding photophysical stability, molar absorptivity measurements showed no significant changes after 4 and 24 hours of irradiation, confirming the compound's resilience under different irradiation conditions. The highest absorptivity was observed in CH_3CN, compared to CH_3OH, indicating the impact of solvent polarity on electronic transitions. A slight shift in maximum wavelength (λ_{max}) after irradiation was recorded, with the largest shift in CH_3CN (-5 nm), followed by CH_3OH (-4 nm), suggesting solvent polarity influences excited-state energy redistribution or induces minor molecular degradation.

Statistical analysis showed that the standard deviation of absorptivity values ranged between ±0.02 and ±0.05, reflecting high reproducibility. No significant outliers or irregular trends were detected, further supporting the reliability of the findings.

These results confirm that $[(tbbpy)_2Ru(tpphz)(PtI_2)_2]$ exhibits high stability under various irradiation and solvent conditions, making it a promising candidate for photocatalysis and solar energy applications. The study also highlights the crucial role of solvent type in determining the compound's spectral properties and stability, with acetonitrile exerting the most pronounced effects.

To further enhance the performance of similar compounds, it is recommended to conduct additional studies on the effects of different temperatures and examine the compound's interaction with other catalysts to improve long-term hydrogen production efficiency.

3.3 Future Work

This study has demonstrated the photostability of ruthenium-based metal complexes and their potential as photocatalysts for solar-driven hydrogen production. However, several areas require further investigation to optimize their efficiency and broaden their applicability.

1. Optimizing ligand structures to improve charge transfer efficiency and catalytic performance.

2. Understanding solvent and environmental effects (polarity, pH, ionic strength).
3. Evaluating electrochemical and catalytic performance in practical hydrogen evolution reactions.
4. Developing hybrid photocatalytic systems to enhance stability and efficiency.

References

Ackermann, M. N., & Interrante, L. V. (1984, November 1). Ruthenium(II) complexes of modified 1,10-phenanthrolines. 1. Synthesis and properties of complexes containing dipyridophenazines and a dicyanomethylene-substituted 1,10-phenanthroline. *Inorg. Chem.*, pp. 3904–3911.

Ahuja, S. (2003). *Chromatography and Separation Science.* Academic Press.

Amouyal, E., Homsi, A., Chambron, J. C., & Sauvage , J. P. (1990). Synthesis and study of a mixed-ligand ruthenium(II) complex in its ground and excited states: bis(2,2′-bipyridine)(dipyrido[3,2-a: 2′,3′-c]phenazine-N4N5)ruthenium(II). *J.Chem.Soc.,DaltonTrans*, pp. 1841-1845.

Armaroli, N., Accorsi, G., Cardinali, F., & Listorti , A. (2007). *Photochemistry and Photophysics of Coordination Compounds I*. Berlin, Springer.

Armaroli, N., & Balzani, V. (2016, January 4). Solar Electricity and Solar Fuels: Status and Perspectives in the Context of the Energy Transition. *Chemistry European Journal*, pp. 32-57.

Atkins, P., Overton, T., Rourke, J., Armstrong, F., & Hagerman, M. (2010). *Shiver & Atkins Inorganic chemistry* (fifth edition ed.). New york: W. H. Freeman.

Badawy, M. I., El-Nouby, M. M., Kimani, P., Lim, L., & Rabea , E. (2022, October 05). A review of the modern principles and applications of solid-phase extraction techniques in chromatographic analysis. *ANAL. SCI.*, pp. 1457–1487.

Balzani, V. (1987). *Supramolecular Photochemistry*. NATO - Science series.

Balzani, V., & Shed, F. (1991). *Supramolecular Photochemistry (Ellis Horwood Series in Physical Chemistry)*. Pearson Education Limited.

Balzani, V. (2001). *Electron Transfer in Chemistry*. WILEY-VCH Verlag GmbH.

Banerjee, T., Haase, F., Savasci, G., Gottschling, K., Ochsenfeld, C., & Lotsch, B. (2017, October 12). Single-Site Photocatalytic H2 Evolution from Covalent Organic Frameworks with Molecular Cobaloxime Co-Catalysts. *J. Am. Chem. Soc.*, pp. 16228–16234.

Bindra, G. S., Schulz, M., Paul, A., Soman, S., Groarke, R., Inglis, J., Vos, J. (2011, Sep 09). The effect of peripheral bipyridine ligands on the photocatalytic hydrogen production activity of Ru/Pdcatalysts. *Dalton Trans*, pp. 10812-10814.

Bindra, G. S., Schulz, M., Paul, A., Groarke, R., Soman, S., Inglis, J., Vos, J. (2012, Jun 18). The role of bridging ligand in hydrogen generation by photocatalytic Ru/Pd assemblies. *Dalton Transactions*, pp. 13050-13059.

Blanchette, S. (2008, February 1). A hydrogen economy and its impact on the world as we know it. *Energy Policy*, pp. 522-530.

Blechschmidt, L., Zedler, L., Mengele, A., Rau, S., & Ivansic, B. (2012, January). Ligand labilization gates intramolecular electron transfer in molecular photocatalyst. The Royal Scociety of Chemistry, pp. 1-3.

Bhusnure, O. G., & Mali, S. (2015, January). RECENT TRENDS IN ION-EXCHANGE CHROMATO- GRAPHY. *International Journal of Drug Policy*, pp. 403-416.

Bo Yin, X., Dong, S., & Wang, E. (2004, June). Analytical applications of theelectrochemiluminescence oftris (2,20-bipyridyl) rutheniumand its derivatives. *TrAC Trends in Analytical Chemistry*, pp. 432-441.

Buchanan, B. E., McGovern, E., Harkin, P., & Vos, J. G. (1988, December 1). The application of high-performance liquid chromatography in the investigation of reactions involving ruthenium(II)bis(bipyridyl) compounds. *Inorg. Chim. Acta*, pp. 1-4.

Buchanan, B. E., Hughes, H., van Diemen, J. H., Hage, R., Haasnoot, J. G., Reedijk, J., & Vos , J. G. (1991). The first report of the isolation and characterisation of an intermediate formed upon photolysis of a ruthenium(II) diimine compound, in which one of the chelating ligands is bound in a monodentate fashion. *J. Chem. Soc., Chem. Commun.*, pp. 300-301.

Bushira, F. A., Hussain, A., Wang, P., Li, H., Zheng, L., Gao, Z., . . . Jin, Y. (2024, May 31). Boosting Electrochemiluminescence Performance of a Dual-Active Site Iron Single-Atom Catalyst-Based Luminol–Dissolved Oxygen System via Plasmon-Induced Hot Holes. *Anal. Chem.*, pp. 9704–9712.

Champness, N. (2011, Sep 02). The future of metal–organic frameworks. *Dalton Trans.*, pp. 10311-10315.

Cheong, W. J., & Carr, P. W. (1990, January 19). Study of partition models in reversed-phase liquid chromatography based on measured mobile phase solute activity coefficients. *Journal of Chromatography A*, pp. 373-393.

Chiorboli, C., Bignozzi, C. A., Scandola, F., Ishow, E., Gourdon, A., & Launay, J. P. (1999, April 28). Photophysics of Dinuclear Ru(II) and Os(II) Complexes Based on the Tetrapyrido[3,2-a:2‘,3‘-c:3‘ ‘,2‘ ‘-h:2‘ ‘‘-3‘ ‘‘-j]phenazine (tpphz) Bridging Ligand. *Inorg. Chem.*, pp. 2402–2410.

Chiorboli, C., Rodgers, M. J., & Scandola, F. (2002, December 4). Ultrafast Processes in Bimetallic Dyads with Extended Aromatic Bridges. Energy and Electron Transfer Pathways in Tetrapyridophenazine-Bridged Complexes. *J. Am. Chem. Soc.*, pp. 483–491.

Chow, J., Kopp, R. J., & Portney, P. R. (2003, Nov 23). Energy Resources and Global Development. *SCIENCE*, pp. 1528-1531.

Clayden, J., Greeves, N., & Warren, S. (2012). *Organic Chemistry*. (s. edition, Ed.) OUP Oxford.

Crosby, G. A. (1975, July 1). Spectroscopic investigation of excited states of transition metal complexes. *Acc.Chem.Res.*, pp. 231-238.

de Silva, A., Fox, D., Huxley, A. M., & Moody, T. (2000, August 1). Combining luminescence, coordination and electron transfer for signalling purposes. *Coordination Chemistry Reviews*, pp. 41-57.

Dini, D., Halpin, Y., Vos, J., & Gibson, E. (2015, December 01). The influence of the preparation method of NiOx photocathodes on the efficiency of p-type dye-sensitized solar cells. *Coordination Chemistry Reviews*, pp. 179-201.

Dolan, J. W. (2002, August 2). Temperature selectivity in reversed-phase high performance liquid chromatography. *Journal of Chromatography A*, pp. 195-205.

Dragull, K., & Beck, J. J. (2012). *Isolation of Natural Products by Ion-Exchange Methods*. Humana Press.

Dürr, H., & Bossmann, S. (2001, October 11). Ruthenium Polypyridine Complexes. On the Route to Biomimetic Assemblies as Models for the Photosynthetic Reaction Center. *Acc. Chem. Res.*, pp 905–917.

Edwards, A. A., & Alexander, B. D. (2017). *Encyclopedia of Spectroscopy and Spectrometry* (Vol. Third Edition). Academic Press.

Etminan, N., & Yoosefian, M. (2016, Jul 04). The role of solvent polarity in the electronic properties, stability and reactivity trend of a tryptophane/Pd doped SWCNT novel nanobiosensor from polar protic to non-polar solvents. *RSC Adv.*, pp. 64818-64825.

Fees, J., Kaim, W., Moscherosch, M., Matheis, W., Klima, J., Krejcik, M., & Zalis, S. (1993, January 1). Electronic structure of the "molecular light switch" bis(bipyridine)dipyrido[3,2-a:2',3'-c]phenazineruthenium(2+). Cyclic voltammetric, UV/visible and EPR/ENDOR study of multiply reduced complexes and ligands. *Inorg. Chem.*, pp. 166–174.

Fujishima, A., & Honda , K. (1972, July 7). Electrochemical Photolysis of Water at a Semiconductor Electrode. *Nature*, pp. 37–38.

Fuquay, J. W. (2011). *Encyclopedia of Dairy Sciences*. Elsevier Ltd.

Gedert, M. H., Nowakowski, M., Kertmen, A., Burkhardt, L., Lindner, N., Schoch, R., . . . Bauer, M. (2021, April 22). Fundamental Characterization, Photophysics andPhotocatalysis of a Base Metal Iron(II)-Cobalt(III) Dyad. *Chemistry - A European Journal*, pp. 9905-9918.

Georg, H. C., Coutinho, K., & Canuto, S. (2007, January 21). Solvent effects on the UV-visible absorption spectrum of benzophenone in water: A combined Monte Carlo quantum mechanics study including solute polarization. *J. Chem. Phys.*

Giddings , J. C. (1965). *Dynamics of Chromatography, Part I: Principles and Theory*. Marcel Dekker.

Gholamkhass, B., Mametsuka, H., Koike, K., Tanabe, T., Furue, M., & Ishitani, O. (2005, March 10). Architecture of Supramolecular Metal Complexes for Photocatalytic CO2 Reduction: Ruthenium−Rhenium Bi- and Tetranuclear Complexes. *Inorg.Chem.*, pp. 2326–2336.

Goldsmith, J., Hudson, W., Lowry, M., Anderson, T., & Bernhard, S. (2005, April 28). Discovery and High-Throughput Screening of Heteroleptic Iridium Complexes for Photoinduced Hydrogen Production. *J. Am. Chem. Soc*, pp. 7502–7510.

Govindarajan, N., Tiwari, A., Ensing, B., & Meijer, E. J. (2018, May 7). Impact of the Ligand Flexibility and Solvent on the O–O Bond Formation Step in a Highly Active Ruthenium Water Oxidation Catalyst. *Inorg. Chem.*, pp. 13063–13066.

Groß , A., Hashimoto, C., Sticht, H., & Eichler , J. (2016, January 19). Synthetic Peptides as Protein Mimics. *Front. Bioeng. Biotechnol.*, pp. 1-16.

Gupta, M. K., & Biswas, P. K. (2023). *Basic Biotechniques for Bioprocess and Bioentrepreneurship*. Elsevier Inc.

Gust, D., Moore, T. A., & Moore, A. L. (1993, Apri 1). Molecular mimicry of photosynthetic energy and electron transfer. *Acc.chem.Res*, pp. 198-205.

Haasnoot, J. G., Hinrichs, W., Weir, O., & Vos, J. G. (1986, November 1). X-ray structure and reactivity of bis(2,2'-bipyridine)carbonylhydridoruthenium hexafluorophosphate hemi(acetone), a possible intermediate in the water-gas shift reaction catalyzed by ruthenium polypyridyl complexes. *Inorg. Chem.* , pp. 4140–4143.

Habermehl, J., Sorsche, D., Murszat, P., & Rau, S. (2016, June 27). Making Use of Obstacles: Alternative Synthetic Approaches towards Osmium(II)-Based Photochemical Molecular Devices. *EurJIC*, pp. 3423-3428.

Halpin, Y., Pryce, M., Rau, S., Dinic, D., & Vos, J. (2013, Sep 26). Recent progress in the development of bimetallic. *Dalton Trans.*,, pp. 16243-16254.

Harcum, S. W. (2008). *Biologically Inspired Textiles.* Woodhead Publishing Series in Textiles.

Harwood, L. M., & Claridge, T. (1996). *Introduction to Organic Spectroscopy* (Vol. 1st Edition). Oxford University Press.

Hasegawa, Y., Nakagawa, T., & Kawai, T. (2010, November). Recent progress of luminescent metal complexes with photochromic units. pp. 2643-2651.

Hatsis, P., & A Lucy, C. (2001, June 22). Effect of temperature on retention and selectivity in ion chromatography of anions. *Journal of Chromatography A*, pp. 3-11.

Heftmann, E. (1975). *Chromatography: A Laboratory Handbook of Chromatographic and Electrophoretic Methods.* Van Nostrand Reinhold.

Hei Yip, A., & Wing Lo, K. (2018, Feb 21). Luminescent rhenium(I), ruthenium(II), and iridium(III) polypyridine complexes containing a poly(ethylene glycol) pendant or bioorthogonal reaction group as biological probes and photocytotoxic agents. *Coordination Chemistry Reviews*, pp. 138-163.

Homocianu, M. (2024, March). Exploring solvatochromism: A comprehensive analysis of research data. *Microchemical Journal*.p.1

Horn, S., Ahmed, H. Y., Hughes, H. P., Soman, S., Browne , W. R., & Vos, J. G. (2010, July 01). Photoinduced ligand isomerisation in a pyrazine-containing ruthenium polypyridyl complex. *Photochemical & Photobiological Sciences*, pp. 985–990.

Iha, N. M. (2000, March). Supramolecular photochemistry and solar cells. *An. Acad. Bras. Ciênc*.

Imanbaew, D., Lang, J., Gelin, M., Kaufhold, S., Pfeffer, M., Rau, S., & Riehn, C. (2017, March 01). Pump-Probe Fragmentation Action Spectroscopy: A Powerful Tool to Unravel Light-Induced Processes in Molecular Photocatalysts. *Angew. Chem.Int. Ed*, pp. 5563-5566.

Inagaki, A., & Akita, M. (2010, June 1). Visible-light promoted bimetallic catalysis. *Coordination Chemistry Reviews*, pp. 1220-1239.

James , P. M., & Gary , W. B. (2006 , 11). Water-Splitting Chemistry of Photosystem II. *American Chemical Society*, pp. 4455–4483.

Jandera, P. (2020). *Handbook of Analytical Separations.* Elsevier B.V.

Johannes , G. V., & Mary, T. P. (2010, November). Photoinduced rearrangements in transition metal compounds. *Coordination Chemistry Reviews*, pp. 2519-2532.

Julià-López, A., Ruiz-Molina, D., Hernando, J., & Roscini, C. (2019, February 28). Solid Materials with Tunable Reverse Photochromism. *ACS Appl. Mater. Interfaces*, pp. 11884–11892.

Juris, A., Balzani, V., Barigelletti, F., Campagna, S., Belser, P., & von Zelewsky , A. (1988, March). Ru(II) polypyridine complexes: photophysics, photochemistry, eletrochemistry, and chemiluminescence. *Chem. Rev*, pp. 85-277.

Kalyanasundaram, K. (1982, January 5). Photophysics, photochemistry and solar energy conversion with tris(bipyridyl)ruthenium(II) and its analogues. *Coordination Chemistry Reviews*, pp. 159-244.

Kalyanasundaram, K. (1992). *Photochemistry of polypyridine and porphyrin complexes.* London: Academic Press.

Karnahl, M., Kuhnt, C., Ma, F., Yartsev, A., Schmitt, M., Dietzek, B., Popp, J. (2011, August 01). Tuning of Photocatalytic Hydrogen Production and Photoinduced Intramolecular Electron Transfer Rates by Regioselective Bridging Ligand Substitution. *ChemPhysChem*, pp. 2101-2109.

Karnahl, M., Kuhnt , C., Heinemann, F., Schmitt, M., Rau, S., Popp, J., & Dietzek, B. (2012, January 17). Synthesis and photophysics of a novel photocatalyst for hydrogen production based on a tetrapyridoacridine bridging ligand. *Chemical Physics*, pp. 65-73.

Kemp, W. (2017). *Organic Spectroscopy* (Vol. 3rd). Bloomsbury Publishing India Pvt. Ltd.

Kenneth, R. S., & Elaine , A. S. (1984). *The Chemistry O f Ruthenium.* Amsterdam: Elsevier Science.

Kenneth , K. W. (2015, July 10). Luminescent Rhenium(I) and Iridium(III) Polypyridine Complexes as Biological Probes, Imaging Reagents, and Photocytotoxic Agents. *American Chemical Society*, pp. 2985–2995.

Kilislioglu, A. (2012). *Ion Exchange Technologies*. InTech.

Kleiman, M., Ah Ryu, K., & Kahn, A. P. (2015, september 10). Determination of factors influuencing the wet etching of polydimethylsiloxane using tetra-n-butylammonium fluoride. *Macromolecular Chemistry and Physics*, pp. 284-291.

Koike, T., & Akita , M. (2014, July 01). Visible-light radical reaction designed by Ru- and Ir-based photoredox catalysis. *Inorg. Chem. Front.*, pp. 562-576.

Komatsuzaki, N., Himeda, Y., Hirose, T., Sugihara, H., & Kasuga, K. (1999, April 1). Synthesis and Photochemical Properties of Ruthenium–Cobalt and Ruthenium–Nickel Dinuclear Complexes. *Bull. Chem. Soc. Jpn*, pp. 725–731.

Lämmle, M., Volk, S., Klinkerman, M., Müßler, M., Mengele, A., & Rau, S. (2022, October 6). Efficient Access of Phenyl-Spaced 5,5′-Bridged Dinuclear Ruthenium Metal Complexes and the Effect of Dynamic Ligand Exchange on Catalysis. *MDPI*, pp. 831-848.

Lehn, J. M. (1988, Jun). Supramolecular Chemistry—Scope and Perspectives Molecules, Supermolecules, and Molecular Devices (Nobel Lecture). *Angew.Chem*, pp. 89-112.

Leppard, J. P., & Reid , E. (1974). Chapter 2. Physical methods and techniques. Part (iv) Chromatography. (a) High-pressure liquid chromatography. *Annu. Rep. Prog. Chem., Sect. B: Org. Chem.*, pp. 44-55.

Lewis, D. E. (2016). *ADVANCED ORGANIC CHEMISTRY.* New York: OUP Oxford.

Lindsay, S. (1992). *High performance liquid chromatography (Analytical Chemistry by Open Learning).* London: Behalf of Thames Polytechnic.

Lincoln, P., Broo, A., & Nordén, B. (1996, Mar 20). Diastereomeric DNA-Binding Geometries of Intercalated Ruthenium(II) Trischelates Probed by Linear Dichroism: [Ru(phen)2DPPZ]2+ and [Ru(phen)2BDPPZ]2+. *J.Am.Chem.Soc*, pp. 2644–2653.

Liu, J., Zhang , S., Wang, W., & Zhang, H. (2023, November). Photoelectrocatalytic principles for meaningfully studying photocatalyst properties and photocatalysis

processes: From fundamental theory to environmental applications. *Journal of Energy Chemistry*, pp. 84-117.

LoBrutto, R., Jones, A., & Kazakevich, Y. (2001, April 13). Effect of counter-anion concentration on retention in high-performance liquid chromatograph

Lombardi, A., Wade, H., Geremia, S., Randaccio, L., Pavone, V., DeGrado, W., & Costanzo, L. (2001, December 19). oward the de Novo Design of a Catalytically Active Helix Bundle: A Substrate-Accessible Carboxylate-Bridged Dinuclear Metal Center. *J. Am. Chem. Soc.* , pp. 12749–12757.

Magdesieva, T. V., & Butin, K. P. (1993, April). Redox potentials and electronic structures of organic complexes of ruthenium and rhodium. *Russ. Chem. Rev*, p. 359.

Marcus, R. A., & Sutin, N. (1985, Agu 1). Electron transfers in chemistry and biology. *Biochimica et Biophysica Acta*, pp. 265-322.

Marcus, R. (1989, April 1). Relation between charge transfer absorption and fluorescence spectra and the inverted region. *J. Phys. Chem.*, pp. 3078–3086.

Marcus, R. (1993, August 01). Electron Transfer Reactions in Chemistry: Theory and Experiment (Nobel Lecture). *Angew. Chem. Int. Ed. Engl.*, pp. 1111-1121.

Matveev, S. M., Mereshchenko, A. S., Panov , M. S., & Tarnovsky, A. N. (2015, February 3). Probing the fate of lowest-energy near-infrared metal-centered electronic excited states: CuCl(4)(2-) and IrBr(6)(2-). *The Journal of Physical Chemistry B*, pp. 4857–4864.

McCalley, D. V. (1996, July 12). Effect of organic solvent modifier and nature of solute on the performance of bonded silica reversed-phase columns for the analysis of strongly basic compounds by high-performance liquid chromatography. *Journal of Chromatography A*, pp. 169-179.

Mengele, A. K., Kaufhold, S., Streb, C., & Rau, S. (2016, Mar 01). Generation of a stable supramolecular hydrogen evolving photocatalyst by alteration of the catalytic center. *Dalton Trans.*, pp. 6612-6618.

Mengele, A. K., & Rau, S. (2022, December 20). Learning from Nature's Example: Repair Strategies in Light-Driven Catalysis. *JACS Au*, pp. 36–46.

Miessler, G., Fischer, P., & Tarr, D. (2013). *Inorganic Chemistry*. Pearson Education.

Mikhnenko, O., Blom, P. M., & Nguyen, T. Q. (2015, May 22). Exciton diffusion in organic semiconductors. *Energy Environ. Sci.*, pp. 1867-1888.

Mistrick, R. G., & Clear, R. (2013, Sep 19). Multilayer Polarizers: A Review of the Claims. *Journal of the Illuminating Engineering Society*, pp. 70-88.

Mora-Diez, N., Montero, L., & Fabian, J. (1998, October 30). Molecular orbital modeling of solvent effects on excited states of organic molecules. *J. Mol. Struct.: THEOCHEM*, pp. 49-57.

Mukherjee, P. K. (2015). *Evidence-Based Validation of Herbal Medicine.* India: Elsevier Inc.

Nagy, P. (1988, December 15). Simple determination of water orientation around hydrated molecules. *Journal of Molecular Structure: THEOCHEM*, pp. 361-375.

Nathan, S. L., & Daniel , G. N. (2006, October 24). Powering the planet: Chemical challenges in solar energy utilization. *The Proceedings of the National Academy of Sciences*, pp. 15729-15735.

Nicolet, Y., Cavazza, C., & Fontecilla-Camps, J. (2002, July 25). Fe-only hydrogenases: structure, function and evolution. *Journal of Inorganic Biochemistry*, pp. 1-8.

Njabon, N. R. (2013, May). An Investigation of the Electronic Coupling in some dimeric ruthenium(II) polypyridine complexes. *Scholarwork@UARK*, p. 1.

Paris, J. P., & Brandt, W. (1959, September 1). Charge Transfer Luminescence of a Ruthenium(ii) Chelate. *J. Am. Chem. Soc.*, pp. 5001–5002.

Pavia, D. L., Lampman, G. M., Kriz, G. S., & Vyvyan, J. R. (2008). *Introduction to Spectroscopy* (vol. Fourth Edition). Cengage Learning.

Pfeffer, M. G., Schäfer, B., Smolentsev, G., Uhlig, J., Nazarenko, E., Guthmuller, J., Kuhnt, C., Wächtler, M., Dietzek, B., Sundström, V., & Rau, S. (2015). Palladium versus platinum: the metal in the catalytic center of a molecular photocatalyst determines the mechanism of the hydrogen production with visible light. *Angewandte Chemie (International ed. in English)*, PP. 5044–5048.

Pfeffer, M. G., Kowacs, T., Wächtler, M., Guthmuller, J., Dietzek, B., Vos, J. G., & Rau, S. (2015, May 26). Optimization of Hydrogen-Evolving Photochemical Molecular Devices. *Angew. Chem., Int. Ed*, pp. 6627-6631.

Pfeffer, M. G., Müller, C., Kastl, E. T. E., Mengele, A. K., Bagemihl, B., Fauth, S. S., Habermehl, J., Petermann, L., Wächtler, M., Schulz, M., Chartrand, D., Laverdière, F., Seeber, P., Kupfer, S., Gräfe, S., Hanan, G. S., Vos, J. G., Dietzek-Ivanšić, B., & Rau, S. (2022). Active repair of a dinuclear photocatalyst for visible-light-driven hydrogen production. *Nature chemistry* . pp. 487–488.

Pharmacia, A. (1999). *Ion Exchange Chromatography Principles.* Amersham Pharmacia Biotech.

Pimputkar, S., Nakamura, S., DenBaars, S. P., & Speck, J. S. (2009, April). Prospects for LED lighting. *Nature Photonics*, pp. 180–182.

Poole, C. (2003, June). New trends in solid-phase extraction. *TrAC Trends in Analytical Chemistry*, pp. 362-373.

Pretsch, E., Bühlmann , P., & Badertscher, M. (2000). *Structure Determination of Organic Compounds.* Berlin: Springer-Verlag.

Pulignani, C., Mesa, C. A., Hillman, S. J., Uekert, T., Giménez, S., Durrant, J. R., & Reisner, E. (2022, December 12). Rational Design of Carbon Nitride Photoelectrodes with High Activity Toward Organic Oxidations .*Angewandte Chemie International Edition.*

Putra, M. H., Bagemihl, B., Rau, S., & Groß, A. (2023, September 27). Prediction of Strong Solvatochromism in a Molecular Photocatalyst. *Weinheim an der Bergstrasse*

Rafferty, J. L., Schure, M. R., & Siepmann , J. I. (2011, April 22). Mobile phase effects in reversed-phase liquid chromatography: A comparison of acetonitrile/water and methanol/water solvents as studied by molecular simulation. *Journal of Chromatography A*, pp. 2203-2213.

Rau, S., Schäfer, B., Anders , E., Rudolph, M., Friedrich , M., Friedrich , M., . . . Vos, J. G. (2006, September 11). A Supramolecular Photocatalyst for the Production of Hydrogen and the Selective Hydrogenation of Tolane. pp. 6215-6218.

Ravisankar, P., Anusha, S., Supriya, K., & Kumar, U. A. (2019, April 02). Fundamental Chromatographic Parameters. *Int. J. Pharm. Sci. Rev. Res.,* , pp. 46 - 50 .

Rotondo, D. (2022, Junuary 01). The fruit fly of photophysics. *Nature Chemistry*, p. 716.

RSC Publishing. (2014). Excited-state reactivity of Ru(II) complexes: Photoinduced ligand dissociation and isomerization. *Dalton Transactions, 43*(41), 15600–15610.

Scandola, F., & Balzani, V. (1991). *Supramolecular Photochemistry.* Ellis Horwood.

Schulz, M., Hirschmann, J., Draksharapu, A., Singh Bindra, G., Soman, S., Paul, A., Groarke, R., Pryce, M. T., Rau, S., Browne, W. R., & Vos, J. G. (2011). Reinvestigating 2,5-di(pyridin-2-yl)pyrazine ruthenium complexes: selective deuteration and Raman spectroscopy as tools to probe ground and excited-state electronic structure in homo-and heterobimetallic complexes. *Dalton transactions*, pp. 10545 - 10552.

Schulz, M., Karnahl, M., Schwalbe, M., & Vos, J. (2012, August). The role of the bridging ligand in photocatalytic supramolecular assemblies for the reduction of protons and carbon dioxide. *Coordination Chemistry Reviews*, pp. 1682-1705.

Schulz, M., Hagmeyer, N., Wehmeyer, F., & Lowe, G. (2020, August 22). Photoinduced Charge Accumulation and Prolonged Multielectron Storage for the Separation of Light and Dark Reaction. *J. Am. Chem. Soc.*, pp. 15722–15728.

Scott , R. P. (1971, August 01). Factors Affecting Peak Capacity in Liquid Chromatography. *Journal of Chromatographic Science*, pp. 449–457.

Semwal, M., Kupfer, S., Zedler, L., Mengele, A., Lammle , M., Brohmer, E., Ivansic, B. (2025, April 10). Role of spacers in Molecularly Linked RuRh Dyads : A Comparative Sunthetic and Ultra spectreoscopic Investigation. *Inorg.Chem*, pp. 7273-7285.

Show, S., & Chattopadhyay, B. (2016, December). Protein Mediated Silica Particles with pH Controlled Porosity and Morphology. *Advances in Microbiology*, pp. 986-998.

Sisk, W. N., Ono, N., Yano, T., & Wada, M. (2002, December 01). Photostability studies of three new bicyclo-boron dipyrromethene difluoride dyes. *Dyes and Pigments*, pp. 143-150.

Singleton, M., Reibenspies, J., & Darensbourg, M. (2010, June 10). A Cyclodextrin Host/Guest Approach to a Hydrogenase Active Site Biomimetic Cavity. *J. Am. Chem. Soc.*, pp. 8870–8871.

Sinval, F. S., Breno, L. S., Cristiane, L. B., & Antonio Otavio , T. P. (2019, Jan 3). Inorganic Photochemistry and Solar Energy Harvesting: Current Developments and Challenges to Solar Fuel Production.*International Journal of Photoenergy*. pp.1-23

Skoog , D., Holler , F. J., & Nieman, T. (1997). *Principles of Instrumental Analysis, 5th Edition 5th Edition*. Brooks Cole.

Skoog, D. A., West, D. M., Crouch, S. R., & Holler, J. (2000). *Analytical Chemistry An introduction* (Vol. 7th ed). Saunders College Pub.

Snyder, L. R., Kirkland, J. J., & Dolan, J. W. (1979). *Introduction to Modern Liquid Chromatography*. New York: John Wiley & Sons, Inc.

Soman, S., Singh Bindra, G., Paul, A., Groarke, R., Manton, J. C., Connaughton, F. M., Schulz, M., Dini, D., Long, C., Pryce, M. T., & Vos, J. G. (2012). Wavelength dependent photocatalytic H2 generation using iridium-Pt/Pd complexes. *Dalton transactions* ,PP.12678–12680

Sun, D. W. (2018). *Modern Techniques for Food Authentication (Second Edition).* Academic Press.

Sunada , Y., Yamaguchi , K., & Suzuki , K. (2022, October 15). “Template synthesis” of discrete metal clusters with two- or three-dimensional architectures. *Coordination Chemistry Reviews*.

Tard, C., Liu, X., Ibrahim, S., Bruschi, M., Gioia, L. D., Davies, S., Pickett, C. (2005, February 09). Synthesis of the H-cluster framework of iron-only hydrogenase. *Nature*, pp. 610–613.

Thauer, R., Klein, A., & Hartmann, G. (1996, November 7). Reactions with Molecular Hydrogen in Microorganisms: Evidence for a Purely Organic Hydrogenation Catalyst. *Chemical Reviews*, pp. 3031–3042.

Twitchett, P. J., & Moffat, A. C. (1975, August 20). High-pressure liquid chromatography of drugs : An evaluation of an octadecylsilane stationary phase. *Journal of Chromatography A*, pp. 149-157.

Valkó, K., Snyder, L. R., & Glajch, J. L. (1993, December 17). Retention in reversed-phase liquid chromatography as a function of mobile-phase composition. *Journal of Chromatography A*, pp. 501-520.

Vidal, L., Riekkola, M. L., & Canals, A. (2012, February 17). Ionic liquid-modified materials for solid-phase extraction and separation: A review. *Analytica Chimica Acta*, pp. 19-41.

Vogler, A., & Kunkely, H. (2000, October). Photochemistry induced by metal-to-ligand charge transfer excitation. *Coordination Chemistry Reviews*, pp. 321-329.

Vogler, A., & Kunkely, H. (2006, July). Photochemistry of peroxo complexes induced by LMCT, MLCT and peroxide IL/LLCT excitation. *Coordination Chemistry Reviews*, pp. 1622-1626.

Ward , M. (1997). Photo-induced electron and energy transfer in non-covalently bonded supramolecular assemblies. *Chem. Soc. Rev.*, pp. 365-375.

Watts, R., & Houten, J. (1974, June 01). Effect of ligand substituents of the d-d luminescence of iridium(III) and rhodium(III) complexes of 1,10-phenanthroline. *J. Am. Chem. Soc.*, pp. 4334–4335.

Webb, G. (1986). *Annual Reports on NMR Spectroscopy.* Academic press: London.

Wellings, D. A. (2006). *A Practical Handbook of Preparative HPLC.* Elsevier.

Weston , A., & Brown, P. (1997). *High Performance Liquid Chromatography & Capillary Electrophoresis: Principles and Practices.* Academic Press.

Wilkinson, G., McCleverty, J., & Gillard, R. D. (1987). *Comprehensive Coordination Chemistry,.* Pergamon Press.

Windle, C. D., & Perutz, R. N. (2012, November). Advances in molecular photocatalytic and electrocatalytic CO2 reduction. *Coord.Chem.Rev*, pp. 2562-2570.

Yang, G., Blechschmidt, L., Zedler, L., Zens, C., Witas, K., Rau, S., Kupfer, S. (2024). Entangled excited state branching processes in a Ru(II)-based push-pull triad. *ChemRxiv*.

Yong Bian, Z., Sumi, K., Furue, M., Sato, S., Koike, K., & Ishitani, O. (2009). Synthesis and properties of a novel tripodal bipyridyl ligand tb-carbinol and its Ru(II)–Re(I) trimetallic complexes: investigation of multimetallic artificial systems for photocatalytic CO2reduction. *Dalton Trans.*, pp. 983-993.

Zanoni, K. S., Kariyazaki, B., Ito, A., Brennaman, M. K., Meyer, T., & Iha, N. M. (2014, March 31). Blue-Green Iridium(III) Emitter and Comprehensive Photophysical Elucidation of Heteroleptic Cyclometalated Iridium(III) Complexes. *Inorg. Chem.*, pp. 4089–4099.

Zedler, L., Wintergerst, P., Mengele, A. K., Müller, C., Li, C., Dietzek-Ivanšić, B., & Rau, S. (2022). Outpacing conventional nicotinamide hydrogenation catalysis by a strongly communicating heterodinuclear photocatalyst. *Nature communications*, P. 2538.

Zhang, J., Wei, Y., Li, H., Zeng, E. Y., & You, J. (2017). Application of Box-Behnken design to optimize multi-sorbent solid phase extraction for trace neonicotinoids in water containing high level of matrix substances. *Talanta*, PP. 392–398.

الخلاصة

تناولت هذه الدراسة تأثير بعض المذيبات على الخواص الطيفية والكيميائية الضوئية لمعقدات الروثينيوم (II) بولي بيريديل، التي تُستخدم على نطاق واسع في تطبيقات تحويل الطاقة الشمسية وإنتاج الهيدروجين. وتهدف إلى تقييم استقرار هذه المعقدات، وانتقال الإلكترونات، وتأثير الإشعاع الضوئي عليها باستخدام تقنيات تحليل متقدمة، مثل كروماتوغرافيا السائل عالية الأداء والتحليل الطيفي للأشعة فوق البنفسجية-المرئية.

في الفصل الأول، تم عرض الخلفية النظرية المتعلقة بالخواص الفيزيائية والكيميائية الضوئية الأساسية لهذه المعقدات، مع التركيز على آليات انتقال الشحنة بين المعدن والليجند (MLCT) ودورها في التحفيز الضوئي. كما تم تحليل تأثير المذيبات في تعديل الديناميكيات الضوئية لهذه المعقدات، مما يسهم في تحسين كفاءتها في التطبيقات التحفيزية.

في الفصل الثاني، تم تفصيل المنهجية التجريبية المتبعة، حيث تمت دراسة معقدات الروثينيوم (II) في مذيبات مختلفة مثل الأسيتونتريل (CH_3CN) ، والميثانول (CH_3OH) ، وثنائي ميثيل السلفوكسيد (DMSO). وقد تم استخدام تقنيات التحليل الطيفي والكروماتوغرافيا لتحديد تأثير هذه المذيبات على الاستقرار الكيميائي الضوئي وسلوك المركبات أثناء التحليل.

أما في الفصل الثالث، فقد تم استعراض النتائج العملية التي كشفت عن تحولات ملحوظة في قمم انتقال الشحنة عند تعريض المركبات للضوء. حيث أظهر المركب $[(tbbpy)_2Ru(tpphz)(PtI_2)_2]$ أعلى امتصاصية موليّة في الأسيتونتريل والميثانول، مع تحول في قمة MLCT من 486 نانومتر إلى 441 نانومتر خلال 24 ساعة، مما يشير إلى حدوث تبادل في الليجندات نتيجة لتفاعل المذيب. كما أظهرت التجارب أن وجود يوديد البلاتين (PtI_2) قد عزز من كفاءة التحفيز الضوئي، حيث سجل هذا المركب معدل إنتاج الهيدروجيني (TON = 276)، مما يعكس تأثير الليجندات على استقرار وأداء النظام التحفيزي.

أظهرت النتائج أيضا أن التغيرات في الامتصاصية المولية كانت ضمن الحدود التجريبية المقبولة، إذ تراوحت قيم الانحراف المعياري بين ±1.1 و±1.5 نانومتر، مع بقاء الانحراف المعياري النسبي (RSD) أقل من 3%، مما يدل على دقة واستقرار القياسات التجريبية. وعند مستوى ثقة 95%، كانت فترات الثقة تشير إلى تغيرات طفيفة في أطوال الموجات القصوى بين 438.9 و446.5 نانومتر، مما يعزز صحة النتائج التجريبية وثبات البيانات المتحصل عليها. تؤكد هذه النتائج أن وسط التفاعل وهيكل الليجندات يلعبان دورًا محوريًا في تحسين أداء معقدات الروثينيوم (II) في التحفيز الضوئي، حيث تُسهم المذيبات عالية القطبية في تعزيز استقرار حالات انتقال الشحنة، مما يزيد من كفاءة التحفيز. بناءً على ذلك، يُوصى بإجراء دراسات إضافية حول تأثير الهياكل الجزيئية المختلفة وظروف التشغيل البيئية على كفاءة وثبات هذه المعقدات، واختبار مذيبات جديدة قد توفر استقرارًا أعلى. بالإضافة إلى ذلك، يُنصح بدمج هذه المعقدات في أنظمة تحفيزية متعددة المكونات لاختبار أدائها في ظروف تشغيل واقعية.

(الكلمات المفتاحية): ***مجمعات الروثينيوم (II) متعددة البيريدين , التحفيز الضوئي ,إنتقال الشحنة من المعدن إلى الرابط (MLCT) , إنتاج الهيدروجين بالطاقة الشمسية , تأثيرات قطبية المذيبات , الاستقرار الضوئي).***